Supporting Information

Artificial Light Harvesting Systems Based on Novel AIEgen-branched Rotaxane Dendrimers for Photocatalyzed Functionalization of C-H Bonds

Xiao-Qin Xu[1], Yi-Ru Song[1], Jiang-Han Cao[1], Wei-Jian Li[1], Yu Zhu[1], Dan-Yang Zhang[1], Wei Wang[1], Xu-Qing Wang[4*], Hai-Bo Yang[123*]

[1]Shanghai Key Laboratory of Green Chemistry and Chemical Processes, State Key Laboratory of Petroleum Molecular and Process Engineering, School of Chemistry and Molecular Engineering, East China Normal University, Shanghai 200062, China

[2]Shanghai Center of Brain-inspired Intelligent Materials and Devices, East China Normal University, Shanghai 200241, China

[3]Shanghai Frontiers Science Center of Molecule Intelligent Syntheses, East China Normal University, Shanghai 200062, China

[4]School of Chemical and Environmental Engineering and Shanghai Engineering Research Center of Green Fluoropharmaceutical Technology, Shanghai Institute of Technology, Shanghai 201418, China

* Corresponding authors.

E-mail: hbyang@chem.ecnu.edu.cn (H.-B. Y.); xqwang@sit.edu.cn (X.-Q. W.)

Table of Contents

Section A. Materials and general methods

All reagents were commercially available and used as supplied without further purification. Deuterated solvents were purchased from Cambridge Isotope Laboratory. Compounds **S1-S2**, **S5-S11** were prepared according to the published procedures.[S1-S2]

All solvents were dried according to standard procedures and all of them were degassed under N_2 for 30 minutes before use. All air-sensitive reactions were carried out under inert N_2 atmosphere. ^{1}H NMR, ^{13}C NMR and ^{31}P NMR spectra were recorded on Bruker 300 MHz Spectrometer (^{1}H: 300 MHz), Bruker 400 MHz Spectrometer (^{1}H: 400 MHz; ^{13}C: 101 MHz, ^{31}P: 162 MHz) and Bruker 500 MHz Spectrometer (^{1}H: 500 MHz; ^{13}C: 126 MHz, ^{31}P: 202 MHz) at 298 K. The ^{1}H and ^{13}C NMR chemical shifts are reported relative to residual solvent signals, and ^{31}P {^{1}H} NMR chemical shifts are referenced to an external unlocked sample of 85% H_3PO_4 (δ 0.0). 2D NMR spectra (^{1}H-^{1}H COSY, ROESY and DOSY) were recorded on Bruker 500 MHz Spectrometer (^{1}H: 500 MHz) at 298 K. The MALDI MS experiments were carried out on a Shimadzu Axima Performance MALDI TOF/TOF Mass Spectrometer, equipped with a 337 nm nitrogen laser. The instrument was operated in positive ion reflectron mode and the accelerating voltage was 20 kV. Electrospray ionization (ESI) mass spectra were recorded with a Waters Synapt G2 mass spectrometer. DLS measurements were performed under a Malvern Zetasizer Nano-ZS light scattering apparatus (Malvern Instruments, U.K.) with a He-Ne laser (633 nm, 4 mW). Transmission electron microscopy (TEM) images were recorded on a Tecnai G2 F30 (FEI Ltd.) at 300 kV. UV-vis spectra and steady-state fluorescence spectra were recorded in a quartz cell (light path 10 mm) on a Shimadzu UV2700 UV-visible spectrophotometer and a Shimadzu RF-6000 fluorescence spectrophotometer. Fluorescence quantum yields were measured in absolutely in solution using a commercial fluorometer with integrating sphere (RF-6000, shimadzu). The fluorescence lifetimes were measured by time correlated single photon counting on a FLS980 instrument (Edinburg Instruments Ltd., Livingstone, UK) with a ^{2}H pulse lamp.

Section B. Synthesis and characterization of [2]rotaxane TPE-R

Scheme S1. The synthesis route of the [2]rotaxane **TPE-R**.

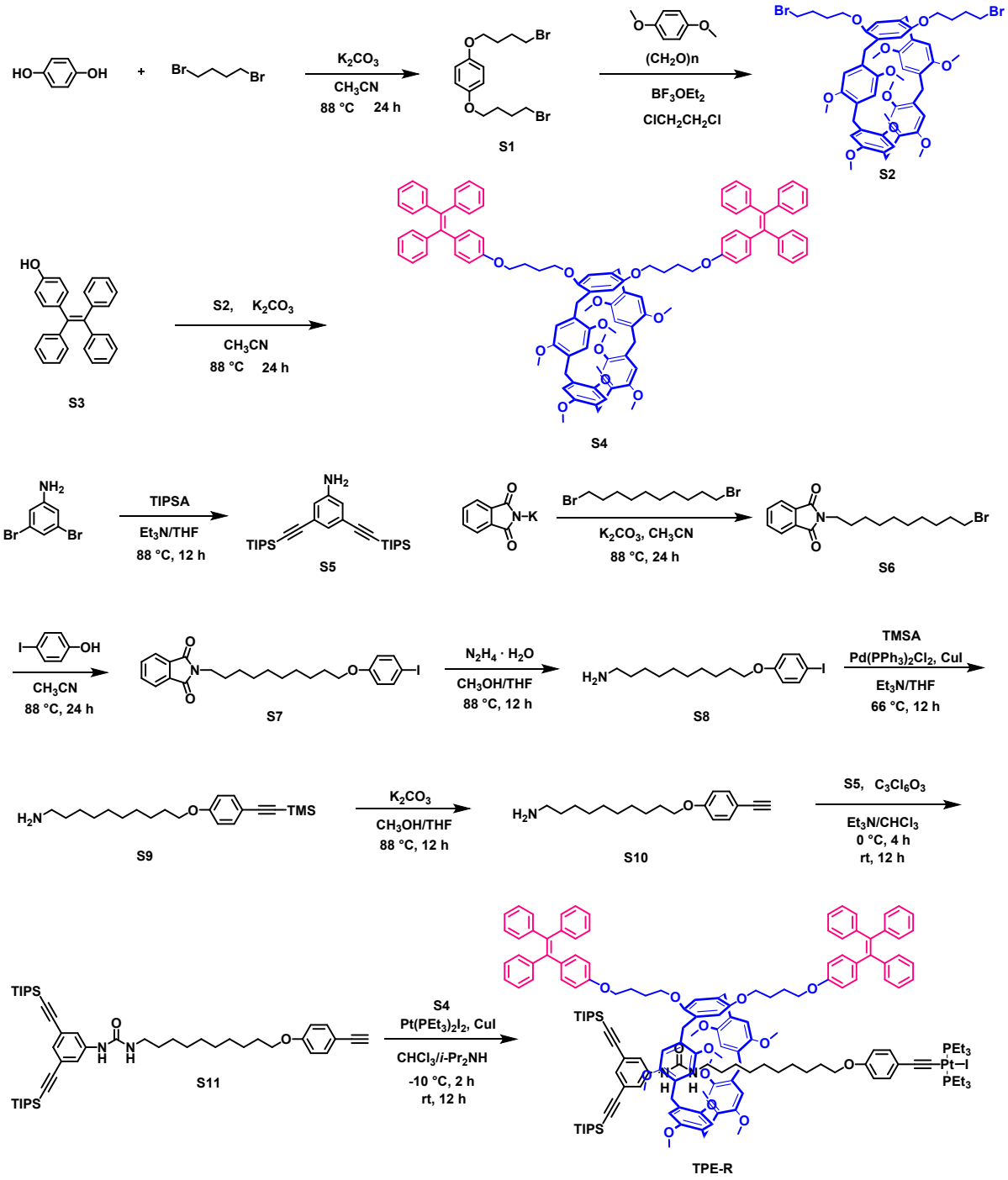

Synthesis of S4: Mixing compound **S3** (2.27 g, 6.51 mmol) and **S2** (1.62 g, 1.63 mmol) in acetonitrile (predried by Na_2SO_4, 100 mL), then K_2CO_3 (1.85 g, 13.4 mmol) was added into the reaction flask. The resultant suspension was refluxed at 88 °C overnight. After cooling to room temperature, the reaction mixture was filtered and the filtrate was concentrated in vacuum. The resultant residue was purified by column chromatography (SiO_2: PE/DCM =2/1) to yield a white solid **S4** (2.2 g, 86.3%). ^{1}H NMR (300 MHz, $CDCl_3$) δ 7.00-7.13 (m, 32H), 6.92-6.95 (d,

J = 9.0 Hz, 4H), 6.75-6.77 (m, 8H), 6.61-6.64 (d, *J* = 9.0 Hz, 4H), 3.59-3.96 (m, 42H), 1.92 (m, 8H). ^{13}C NMR (101 MHz, $CDCl_3$) δ 157.60, 150.70, 150.65, 149.82, 144.12, 144.06, 144.04, 140.58, 140.17, 136.19, 132.65, 131.46, 131.43, 131.41, 128.39, 128.36, 128.33, 128.26, 127.82, 127.69, 126.45, 126.35, 126.32, 114.60, 113.94, 113.92, 113.87, 113.81, 113.57, 67.91, 67.38, 55.85, 55.83, 55.80, 52.89, 29.60, 29.53, 29.45, 26.62, 26.46. HRMS (ESI-TOF-MS) *m/z* = 1527.7131 [**S4** + H]$^+$ ($C_{103}H_{99}O_{12}^+$ requires 1527.7132).

Synthesis of [2]rotaxane TPE-R: A Schlenk flask was charged with macrocycle **S4** (3.2 g, 2.09 mmol), thread component **S11** (263 mg, 0.35 mmol) and $Pt(PEt_3)_2I_2$ (956.5 mg, 1.4 mmol). The Schlenk flask was then evacuated and back-filled with N_2 three times. Next, the mixture solvent of degassed $CHCl_3$ and *i*-Pr_2NH (v/v, 20/10 mL) was added. The resultant solution was stirred for 2 h under -10 °C. Then a catalytic amount of CuI (6.7 mg) was added to the mixture under an inert atmosphere. Then the reaction mixture was allowed to warm to room temperature and stirred overnight. The solution was concentrated and the residue was purified by column chromatography (SiO_2: PE/DCM) and preparative gel permeation chromatography (GPC). A white solid **TPE-R** was obtained (720 mg, 70.0%). ^{1}H NMR (400 MHz, CD_2Cl_2): δ 7.59 (d, *J* = 0.8 Hz, 2H), 7.17-7.22 (m, 3H), 7.00-7.12 (m, 35H), 6.85-6.96 (m, 10H), 6.77-6.79 (d, *J* = 8.0Hz, 2H), 6.64-6.67 (d, *J* = 12.0 Hz, 2H), 6.58-6.60 (d, *J* = 8.0Hz, 2H), 3.73-4.00 (m, 44H), 2.46 (m, 1H), 1.82-2.25 (m, 20H), 1.65-1.72 (m, 2H), 1.12-1.38 (m, 64H), 0.84-0.89 (m, 2H), 0.69-0.77 (m, 2H), 0.59 (m, 2H), -0.04-0.04 (m, 2H), -1.50-(-1.43) (m, 2H), -2.03-(-1.94) (m, 2H). ^{13}C NMR (101 MHz, CD_2Cl_2): δ 159.73, 159.70, 159.20, 159.14, 157.23, 153.27, 150.98, 150.68, 150.61, 150.56, 50.39, 150.35, 150.24, 149.86, 149.85, 149.84, 140.81, 137.05, 136.91, 136.88, 136.85, 132.89, 132.80, 132.73, 132.69, 131.68, 130.16, 130.14, 130.12, 129.91, 129.60, 129.26, 128.77, 128.54, 128.44, 128.40, 128.34, 128.33, 128.30, 128.10, 127.81, 127.77, 127.71, 127.45, 126.52, 126.49, 126.44, 125.12, 125.08, 125.06, 124.00, 122.82, 122.78, 122.75, 122.49, 114.72, 114.70, 114.57, 114.56, 114.23, 114.15, 113.11, 106.41, 90.89, 68.51, 68.03, 67.91, 67.83, 67.77, 57.10, 56.50, 56.34, 56.25, 55.38, 55.35, 53.97, 53.70, 53.43, 53.16, 52.89, 39.31, 30.99, 30.51, 30.08, 30.07, 29.69, 29.51, 29.15, 29.03, 26.79, 26.65, 26.54, 26.41, 26.20, 25.18, 18.47, 16.77, 16.59, 16.41, 11.34, 8.04. ^{31}P NMR (162 MHz, CD_2Cl_2): δ 8.74. HRMS (ESI-TOF-MS) *m/z* = 2838.2734 [**TPE-R** + H]$^+$ ($C_{162}H_{200}IN_2O_{14}P_2PtSi_2^+$ requires 2838.2734).

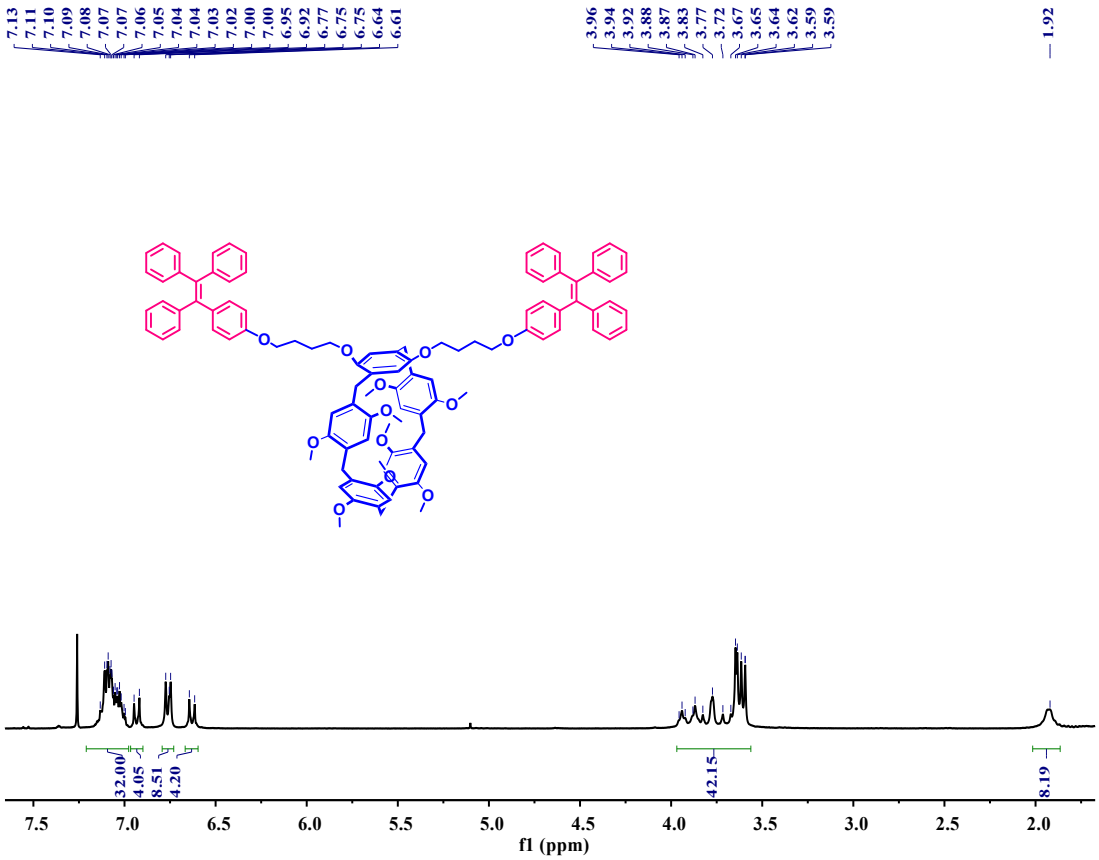

Figure S1. ^{1}H NMR spectrum (300 MHz, 298 K, $CDCl_3$) of **S4**.

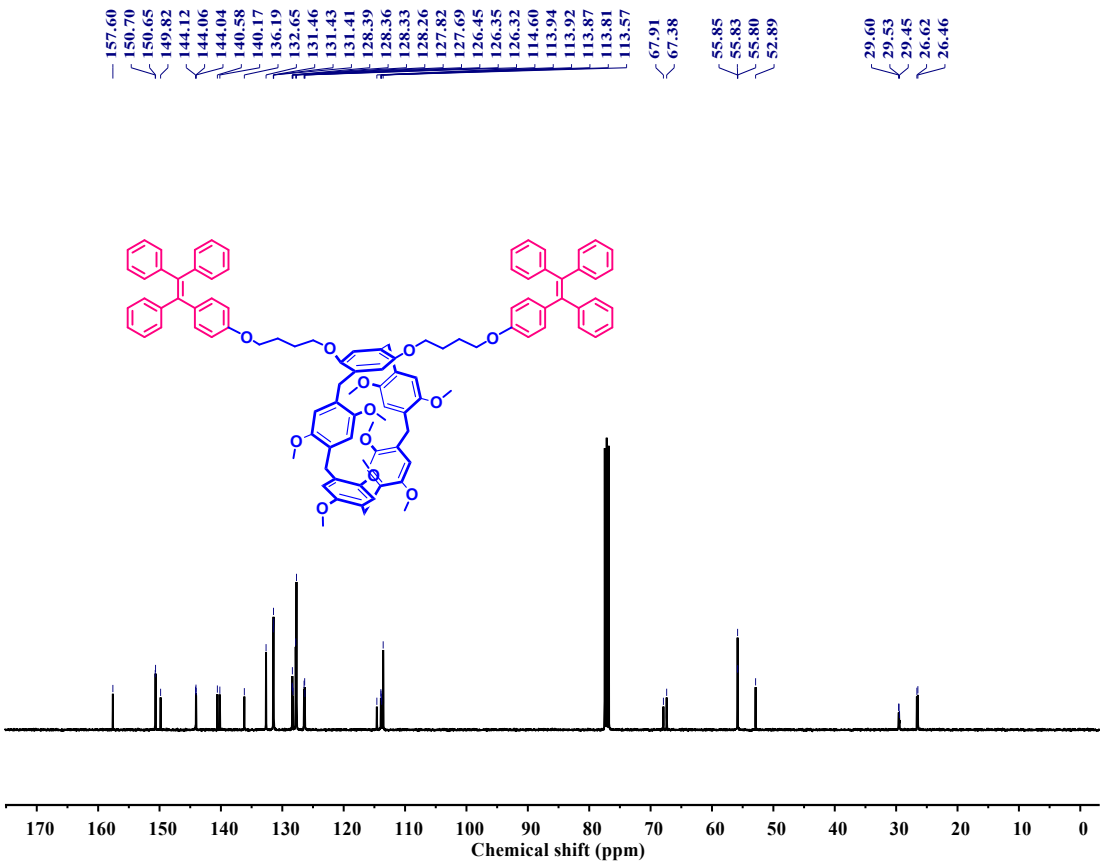

Figure S2. ^{13}C NMR spectrum (101 MHz, 298 K, $CDCl_3$) of **S4**.

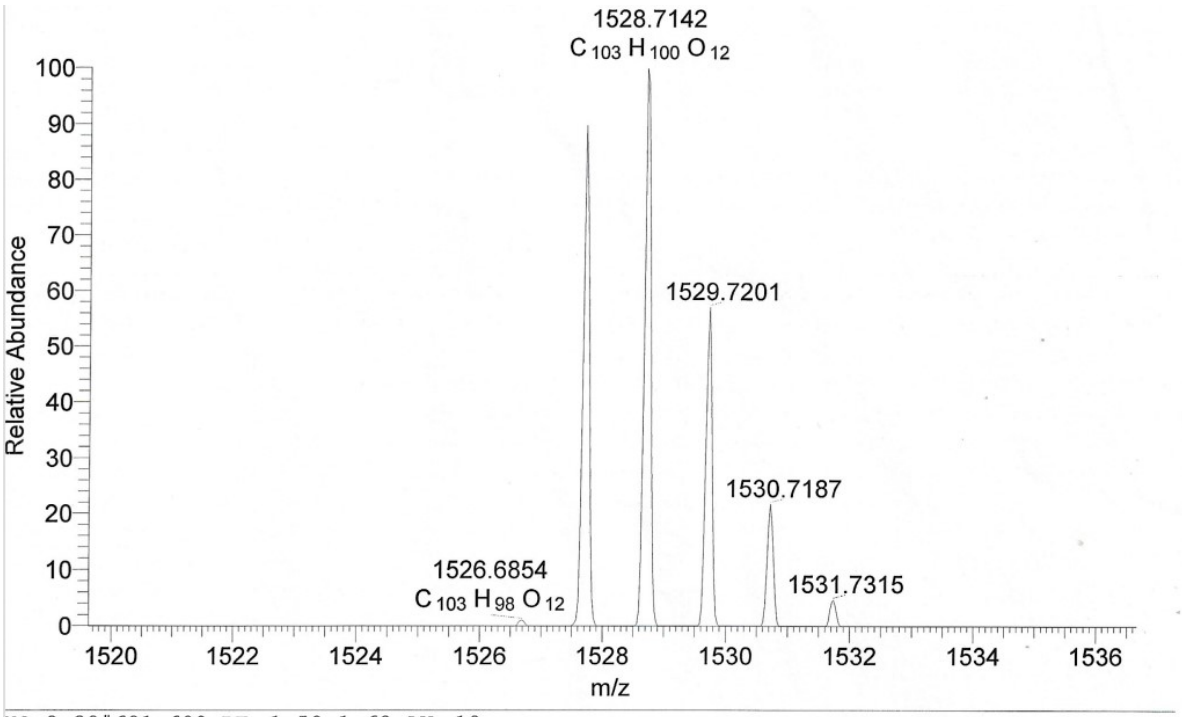

XQ-2-38#681-698 RT: 1.58-1.62 AV: 18
B: 378 0.93-1.52 , 1.79-2.08
: FTMS + p ESI Full ms [150.0000-2000.0000]
/z= 1519.6264-1536.6577

m/z	Intensity	Relative	Theo. Mass	Delta (ppm)	RDB equiv.	Composition
1526.6854	17391.5	1.03	1526.7053	-19.86	55.0	$C_{103}H_{98}O_{12}$
1527.7131	1474671.6	87.54	1527.7131	0.03	54.5	$C_{103}H_{99}O_{12}$
1528.7142	1684494.0	100.00	1528.7209	-6.78	54.0	$C_{103}H_{100}O_{12}$
1529.7201	939401.3	55.77				
1530.7187	357943.1	21.25				
1531.7315	77250.8	4.59				

Figure S3. HRMS (ESI-TOF-MS) spectrum of **S4**.

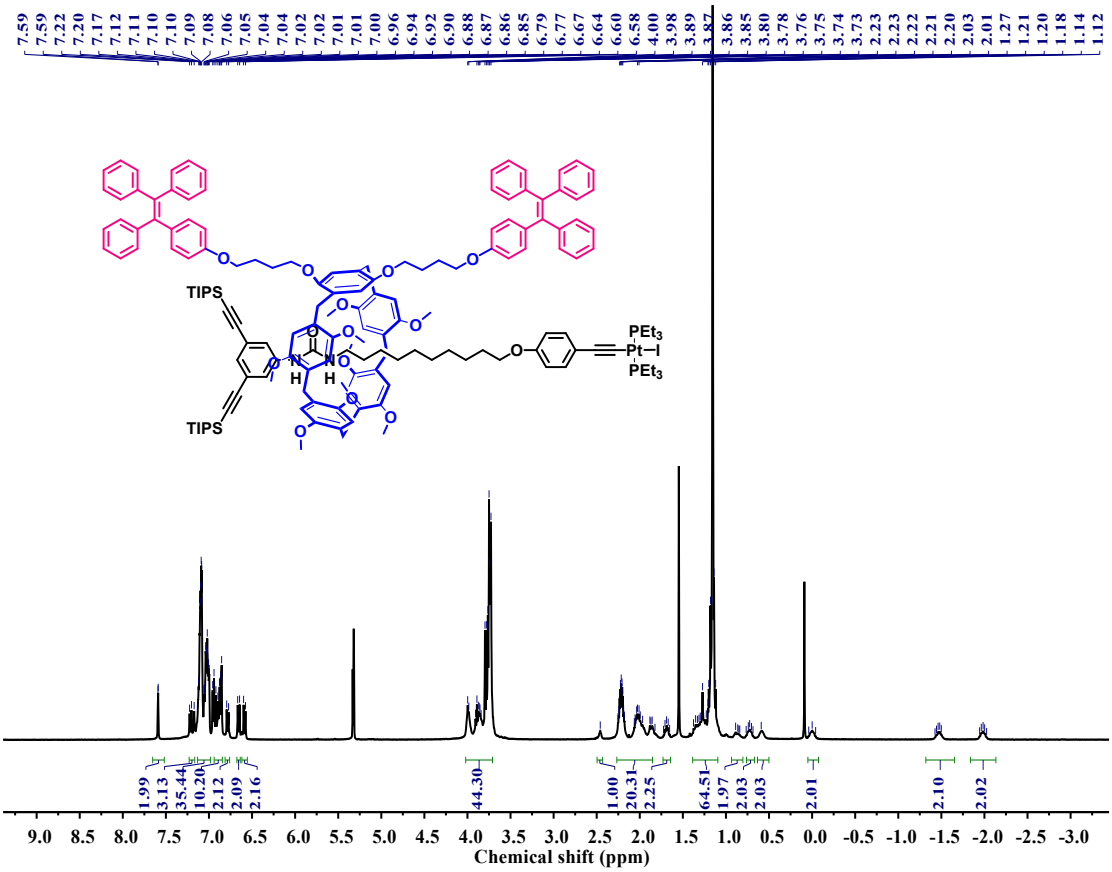

Figure S4. ^{1}H NMR spectrum (400 MHz, 298 K, CD_2Cl_2) of [2]rotaxane **TPE-R**.

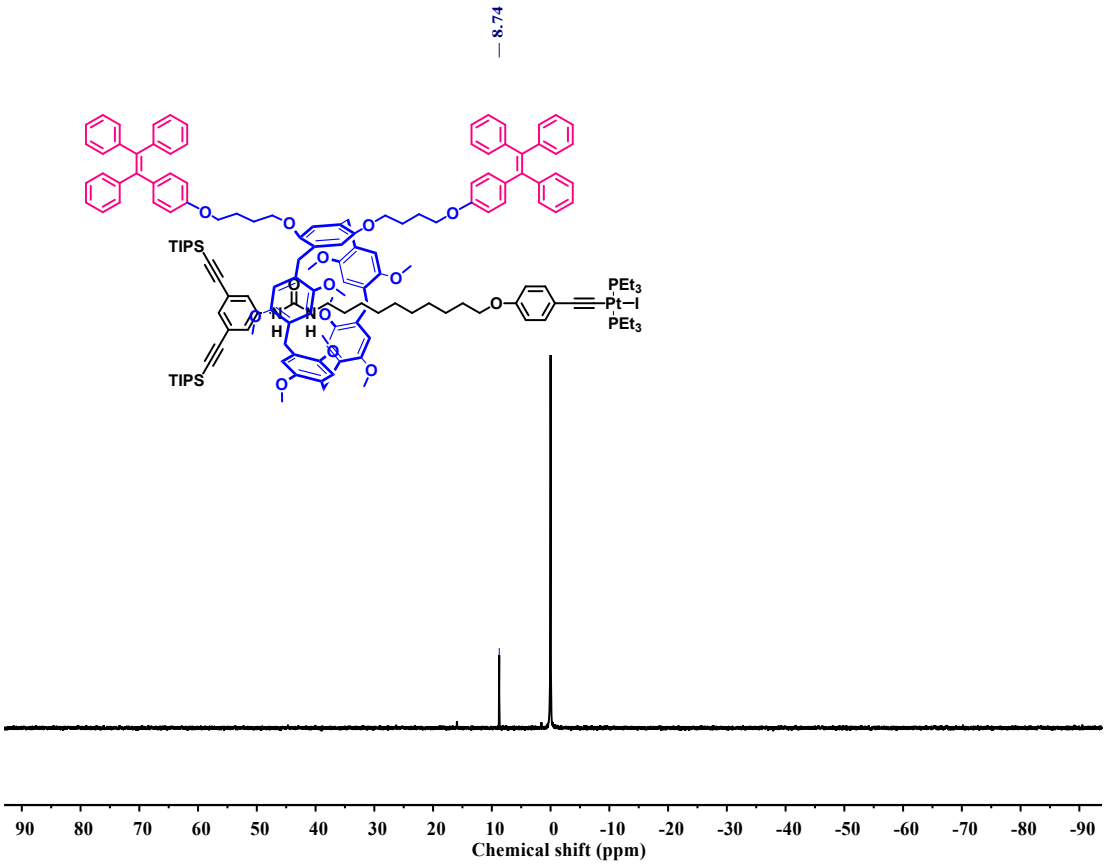

Figure S5. ^{31}P NMR spectrum (162 MHz, 298 K, CD_2Cl_2) of [2]rotaxane **TPE-R**.

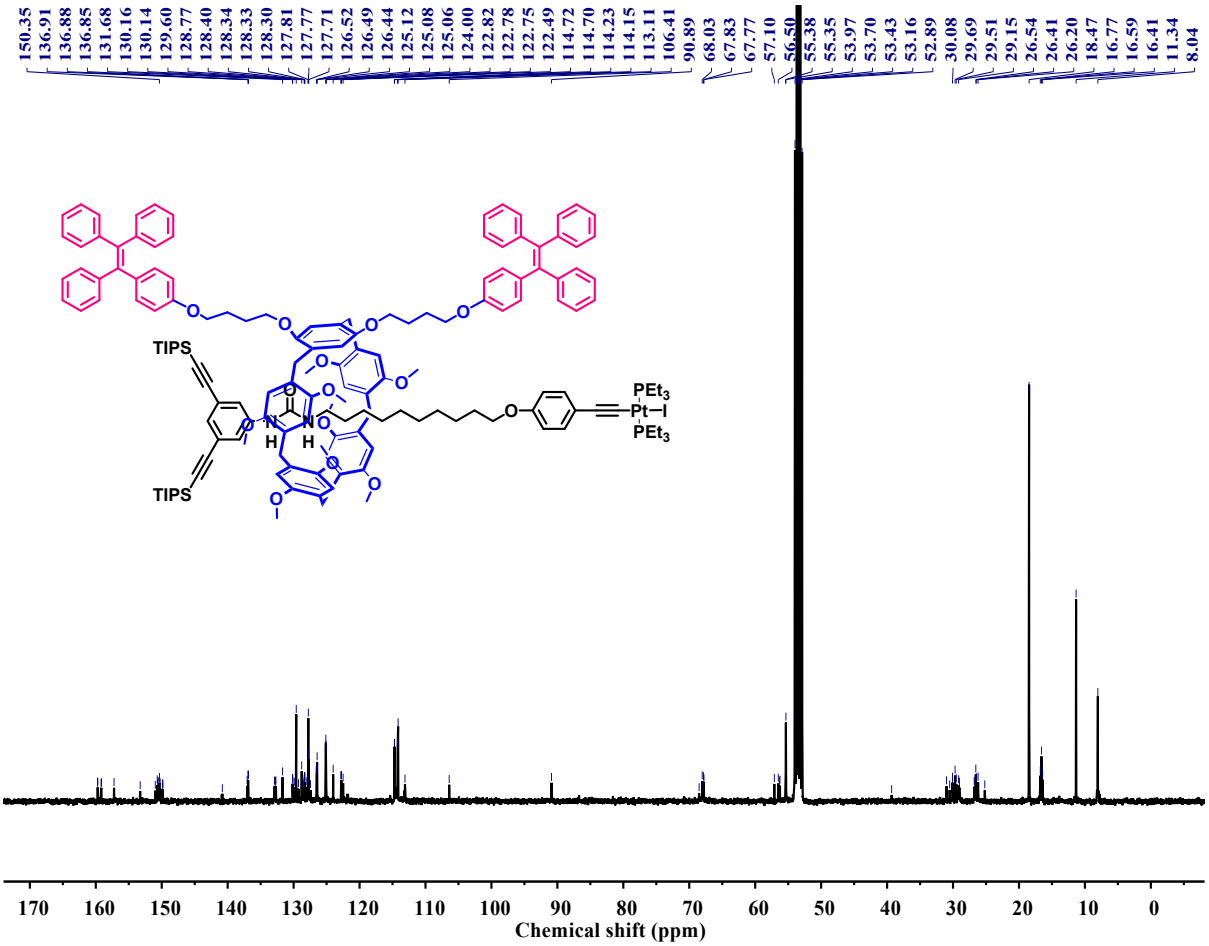

Figure S6. ^{13}C NMR spectrum (101 MHz, 298 K, CD_2Cl_2) of [2]rotaxane **TPE-R**.

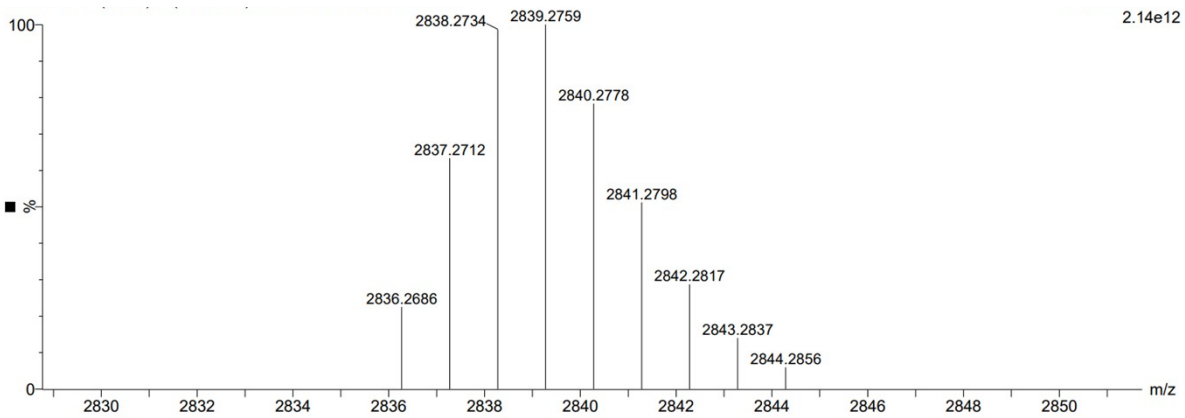

Figure S7. HRMS (ESI-TOF-MS) spectrum of [2]rotaxane **TPE-R**.

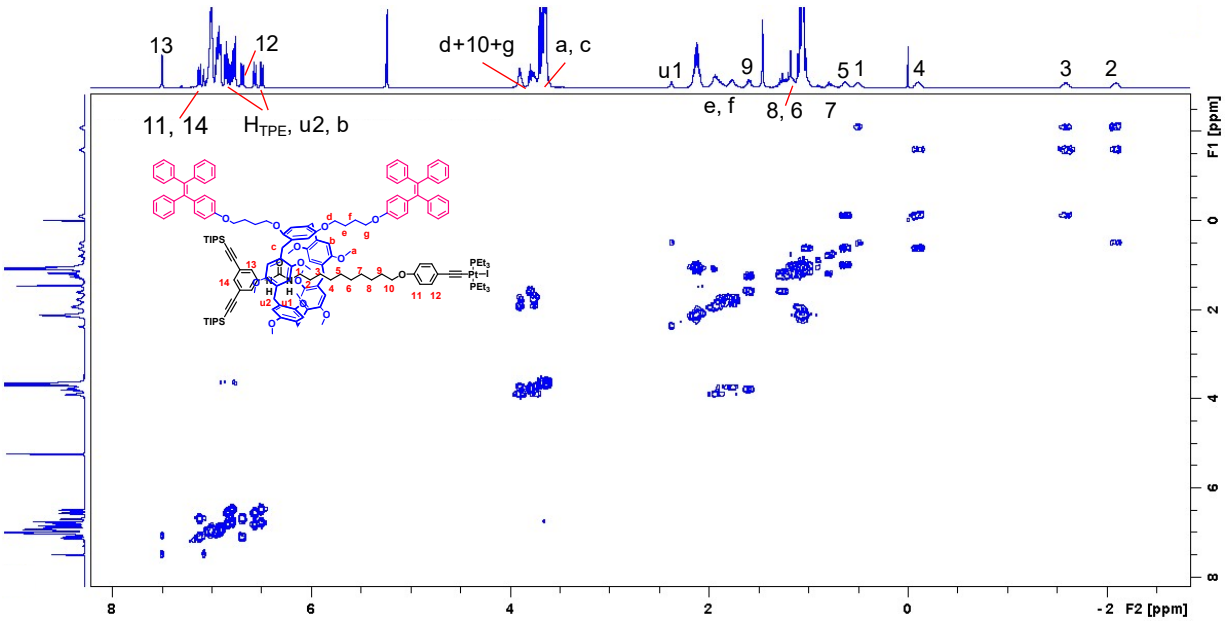

Figure S8. 2D ^{1}H-^{1}H COSY spectrum (CD_2Cl_2, 298 K, 500 MHz) of [2]rotaxane **TPE-R**.

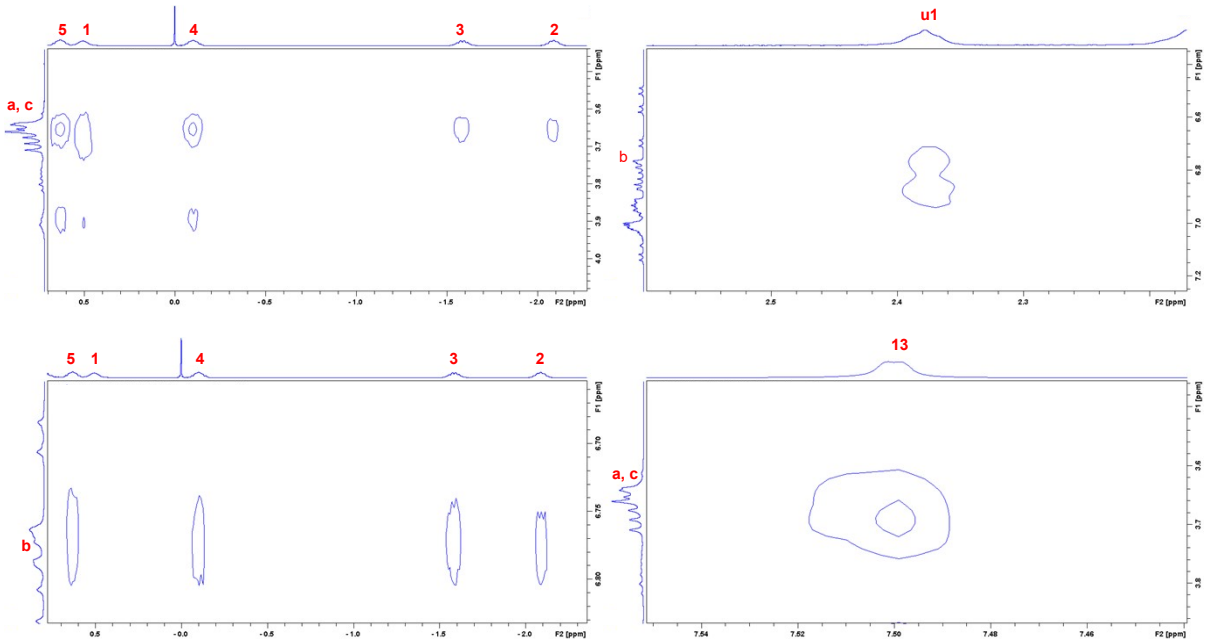

Figure S9. 2D ^{1}H-^{1}H ROESY spectra (CD_2Cl_2, 298 K, 500 MHz) of [2]rotaxane **TPE-R**.

Section C. Synthesis and characterization of rotaxane dendrimers TPE-Gn (n = 1, 2, 3)

Synthesis of the first-generation rotaxane dendrimer TPE-G1.

Scheme S2. Synthesis route of the rotaxane dendrimer **TPE-G1**.

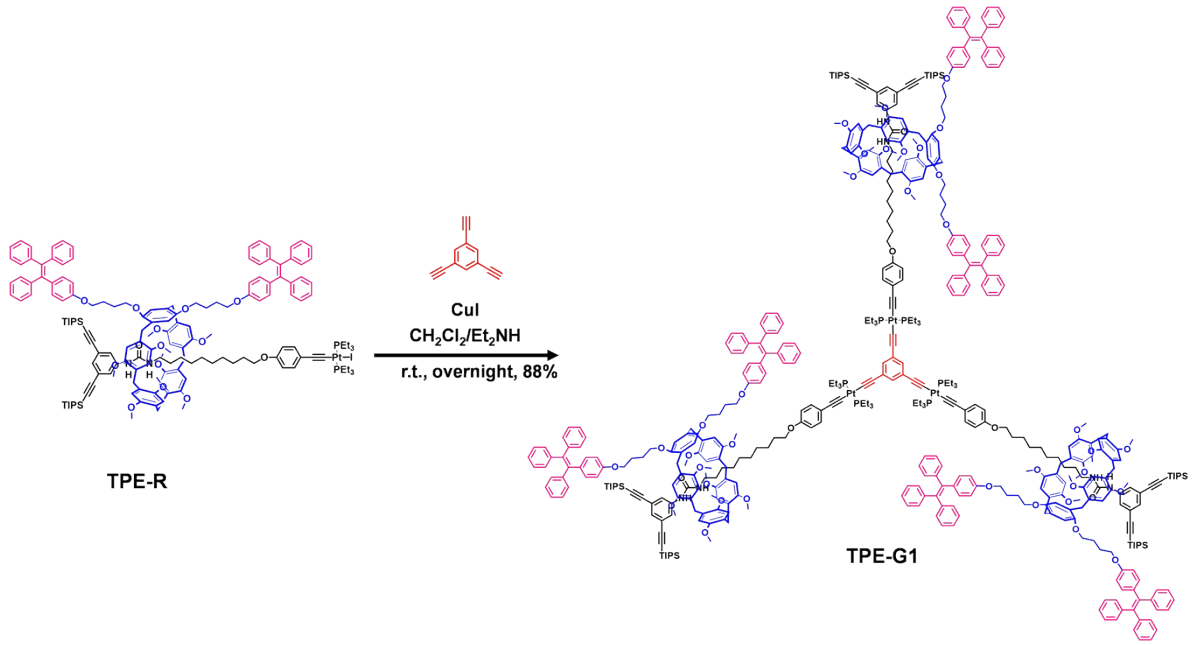

Synthesis of the first-generation rotaxane dendrimer TPE-G1: A mixture of 1,3,5-tris(4-ethynylphenyl)benzene (4.0 mg, 0.027 mmol) and [2]rotaxane **TPE-R** (249.5 mg, 0.088 mmol) were added in a Schlenk flask, the Schlenk flask was then evacuated and back-filled with N_2 three times. Next, the degassed Et_2NH and CH_2Cl_2 (v/v, 2/2 mL) and a catalytic amount of CuI (1.67 mg) was added under an inert atmosphere. The reaction was stirred overnight at room temperature. The solvent was evaporated and the residue was purified by column chromatography (SiO_2; PE/DCM) and preparative gel permeation chromatography (GPC) to yield a white solid **TPE-G1** (194 mg, 88%). ^{1}H NMR (400 MHz, CD_2Cl_2): δ 7.60 (m, 6H), 6.87-7.22 (m, 148H), 6.77-6.79 (d, J = 8.0 Hz, 6H), 6.66-6.68 (d, J = 8.0 Hz, 6H), 6.58-6.61 (d, J = 12.0 Hz, 6H), 3.74-4.01 (m, 130H), 2.49 (m, 3H), 1.83-2.22 (m, 60H), 1.66-1.73 (m, 6H), 1.16-1.27 (m, 198H), 0.69-0.77 (m, 6H), 0.62 (m, 6H), -0.04-0.04 (m, 6H), -1.51-(-1.46) (m, 6H), -2.02-(-1.94) (m, 6H). ^{13}C NMR (101 MHz, CD_2Cl_2): δ 157.82, 157.79, 157.02, 153.34, 151.05, 150.72, 150.68, 150.63, 150.46, 150.42, 150.38, 150.27, 149.89, 149.86, 144.26, 144.22, 144.19, 144.15, 144.14, 140.84, 140.70, 140.24, 140.05, 136.13, 135.87, 132.52, 132.42, 131.94, 131.38, 131.34, 131.31, 131.29, 131.27, 129.34, 128.82, 128.79, 128.60, 128.46, 128.39, 127.80, 127.79, 127.69, 127.66, 127.64, 126.43, 126.37, 126.35, 126.33, 126.24, 124.04, 121.86, 121.52, 115.43, 114.60, 114.55, 114.39, 114.30, 114.20, 113.57, 113.55, 113.20, 106.50, 90.92, 68.58, 68.08, 67.93, 67.58, 67.52, 57.20, 56.54, 56.40, 56.31,

55.45, 55.44, 55.41, 54.10, 53.96, 39.38, 31.08, 30.60, 30.16, 30.13, 29.59, 29.24, 29.21, 29.09, 26.85, 26.72, 26.63, 26.48, 26.29, 25.26, 18.59, 16.63, 16.46, 16.29, 11.44, 8.27. ^{31}P NMR (162 MHz, CD_2Cl_2): δ 11.72. LRMS (MALDI-TOF) *m/z* = 8282.2 [**TPE-G1** + H]$^+$ ($C_{498}H_{601}N_6O_{42}P_6Pt_3Si_6^+$ requires 8282.9).

Synthesis of the second-generation rotaxane dendrimer TPE-G2.

Scheme S3. Synthesis route of the rotaxane dendrimer **TPE-G2**.

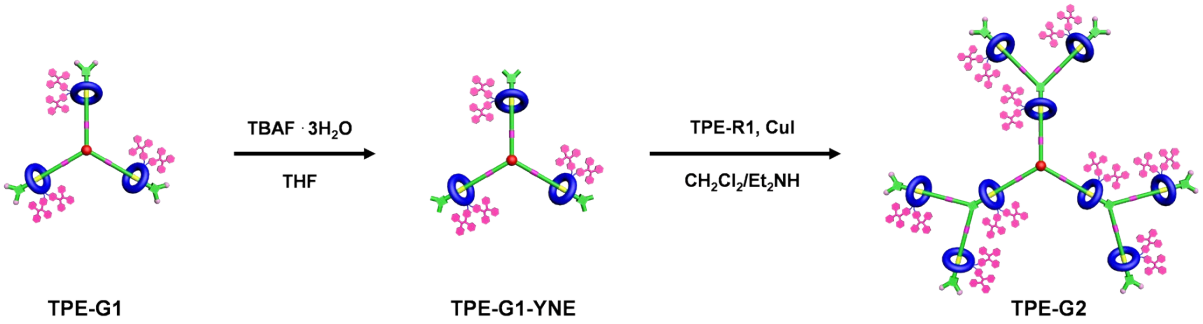

Synthesis of the rotaxane dendrimer TPE-G2: A reaction flask was charged with a THF solution of **TPE-G1** (120 mg, 0.0133 mmol) and then a solution of $Bu_4NF{\cdot}3H_2O$ (50.3 mg, 0.16 mmol) in THF was added dropwise into the reaction flask. The reaction mixture was stirred at room temperature for 2 h, the obtained residue was washed by water, then dried with Na_2SO_4 and concentrated. The residue was further purified by column chromatography (SiO_2; DCM) and preparative gel permeation chromatography (GPC) to afford a pale yellow solid **TPE-G1-YNE** (106 mg). Then the obtained **TPE-G1-YNE** and [2]rotaxane **TPE-R** (270 mg, 0.09 mmol) were added in a Schlenk flask, the Schlenk flask was then evacuated and back-filled with N_2 three times. Next, the degassed Et_2NH and CH_2Cl_2 (v/v, 2/2 mL) and a catalytic amount of CuI were added under an inert atmosphere. The reaction was stirred overnight at room temperature. The solvent was evaporated and the residue was purified by column chromatography (SiO_2; DCM/EA) and preparative gel permeation chromatography (GPC) to yield a pale yellow solid **TPE-G2** (245 mg, 72%). ^{1}H NMR (400 MHz, CD_2Cl_2): δ 7.59 (m), 6.85-7.21 (m), 6.75-6.78 (m), 6.57-6.67 (m), 3.72-4.00 (m), 2.86 (m), 2.47-2.49 (m), 2.14-2.21 (m), 1.81-2.03 (m), 1.64-1.72 (m), 1.15-1.27 (m), 0.98 (m), 0.68-0.76 (m), 0.59 (m), -0.05-0.04 (m), -0.16 (m), -1.50-(-1.44) (m), -1.62 (m), -2.01-(-1.86) (m). ^{13}C NMR (101 MHz, CD_2Cl_2): δ 158.28, 158.25, 158.22, 157.48, 153.80, 151.47, 151.15, 151.11, 151.06, 151.00, 150.89, 150.85, 150.81, 150.70, 150.32, 150.29, 144.69, 144.65, 144.62, 144.59, 144.57, 141.27, 141.13, 140.67, 140.48, 136.56, 136.32, 136.30, 132.96, 132.88, 132.85, 132.38, 131.81, 131.77, 131.74, 131.72, 131.71, 129.76, 129.25, 129.22, 129.03, 128.89, 128.82, 128.23, 128.22, 128.12, 128.10, 128.07, 126.87, 126.80, 126.79, 126.76, 126.67, 124.46, 115.85, 115.03, 114.96,

114.81, 114.71, 114.63, 114.60, 114.07, 114.00, 113.98, 113.61, 106.94, 91.34, 69.00, 68.58, 68.52, 68.36, 68.02, 67.95, 57.62, 56.96, 56.82, 56.73, 56.59, 55.89, 55.87, 55.84, 54.40, 39.79, 31.51, 31.04, 30.59, 30.03, 29.67, 29.65, 29.56, 27.28, 27.19, 27.06, 26.89, 26.79, 26.72, 25.71, 19.02, 17.12, 17.07, 16.95, 16.90, 16.77, 16.72, 11.87, 8.75, 8.71. ^{31}P NMR (162 MHz, CD_2Cl_2): δ 11.94, 11.83. LRMS (MALDI-TOF) *m/z* = 23639.8 [**TPE-G2**]$^+$ ($C_{1418}H_{1676}N_{18}O_{126}P_{18}Pt_9Si_{12}^+$ requires 23639.3).

Synthesis of the third-generation rotaxane dendrimer TPE-G3.

Scheme S4. Synthesis route of the rotaxane dendrimer **TPE-G3**.

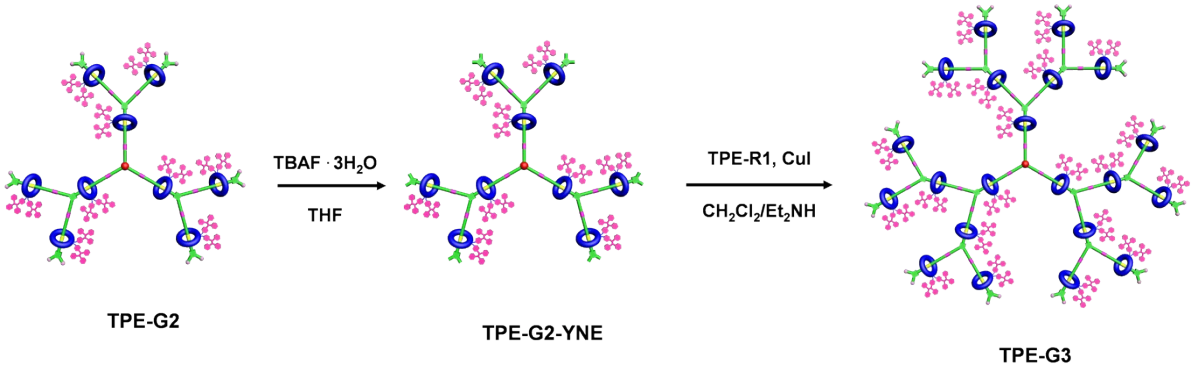

Synthesis of the rotaxane dendrimer TPE-G3: A reaction flask was charged with a THF solution of **TPE-G2** (145 mg, 0.0061 mmol) and then a solution of $Bu_4NF{\cdot}3H_2O$ (46.4 mg, 0.147 mmol) in THF was added dropwise into the reaction flask. The reaction mixture was stirred at room temperature for 2 h, the obtained residue was washed by water, then dried with Na_2SO_4 and concentrated. The residue was further purified by column chromatography (SiO_2; DCM/EA) and preparative gel permeation chromatography (GPC) to afford a pale yellow solid **TPE-G2-YNE** (133 mg). Then, the obtained **TPE-G2-YNE** and [2]rotaxane **TPE-R** (231 mg, 0.081 mmol) were added in a Schlenk flask, the Schlenk flask was then evacuated and back-filled with N_2 three times. Next, the mixture solvent of the degassed Et_2NH and CH_2Cl_2 (v/v, 2/2 mL) was added via syringe. Subsequently, a catalytic amount of CuI was added under an inert atmosphere. The reaction was stirred overnight at room temperature. The solvent was evaporated and the residue was purified by column chromatography (SiO_2; DCM/EA) and preparative gel permeation chromatography (GPC) to yield a pale yellow solid **TPE-G3** (259 mg, 78%). ^{1}H NMR (400 MHz, CD_2Cl_2): δ 7.59-7.60 (m), 6.86-7.22 (m), 6.77-6.79 (m), 6.58-6.67 (m), 3.73-4.00 (m), 2.86 (m), 2.48 (m), 2.16-2.21 (m), 1.83-2.04 (m), 1.65-1.72 (m), 1.16-1.28 (m), 0.99-1.00 (m), 0.69-0.77 (m), 0.60 (m), 0.00 (m), -0.15 (m), -1.49-(-1.44) (m), -1.61 (m), -2.01-(-1.89) (m). ^{13}C NMR (101 MHz, CD_2Cl_2): δ 157.89, 157.86, 157.82, 157.06,

153.35, 151.09, 150.75, 150.72, 150.67, 150.58, 150.51, 150.47, 150.43, 150.32, 149.92, 144.28, 144.24, 144.21, 144.17, 144.16, 140.87, 140.73, 140.28, 140.08, 136.16, 135.92, 135.89, 132.53, 132.46, 132.44, 132.43, 131.95, 131.39, 131.35, 131.32, 131.30, 131.28, 129.37, 128.86, 128.83, 128.64, 128.51, 128.44, 127.81, 127.80, 127.70, 127.67, 126.45, 126.38, 126.36, 126.34, 126.25, 124.06, 115.47, 114.44, 114.39, 114.35, 114.24, 114.21, 113.68, 113.61, 113.59, 113.26, 106.55, 90.93, 68.61, 68.19, 68.13, 67.98, 67.63, 67.56, 57.21, 56.55, 56.42, 56.33, 56.18, 55.49, 55.47, 55.44, 54.03, 54.03, 39.37, 31.08, 30.61, 30.17, 30.16, 29.63, 29.29, 29.24, 29.15, 26.87, 26.76, 26.65, 26.50, 26.38, 26.31, 25.30, 18.60, 16.74, 16.57, 16.40, 11.47, 8.34, 8.29. ^{31}P NMR (162 MHz, CD_2Cl_2): δ 11.80.

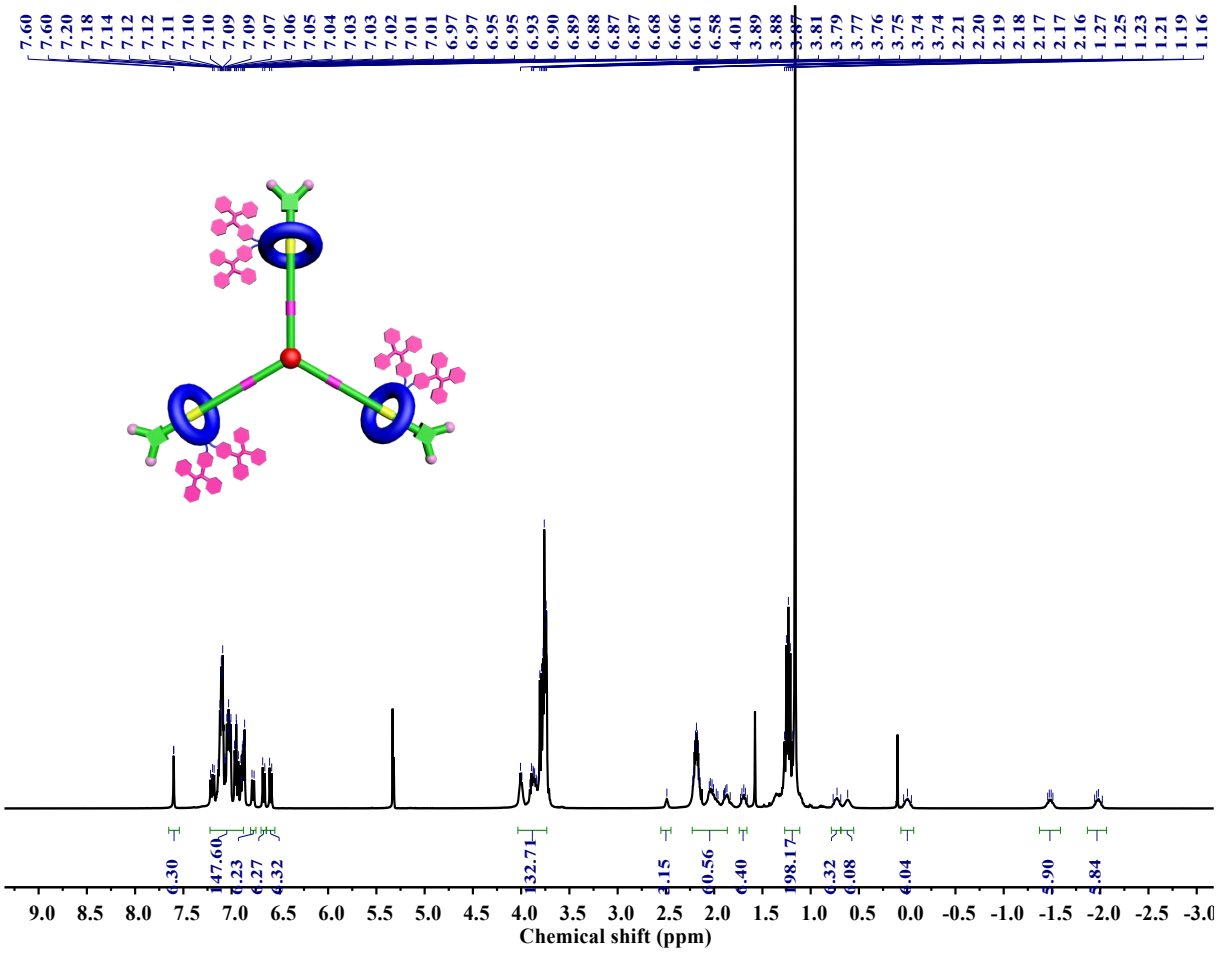

Figure S10. ^{1}H NMR spectrum (CD_2Cl_2, 298 K, 400 MHz) of **TPE-G1**.

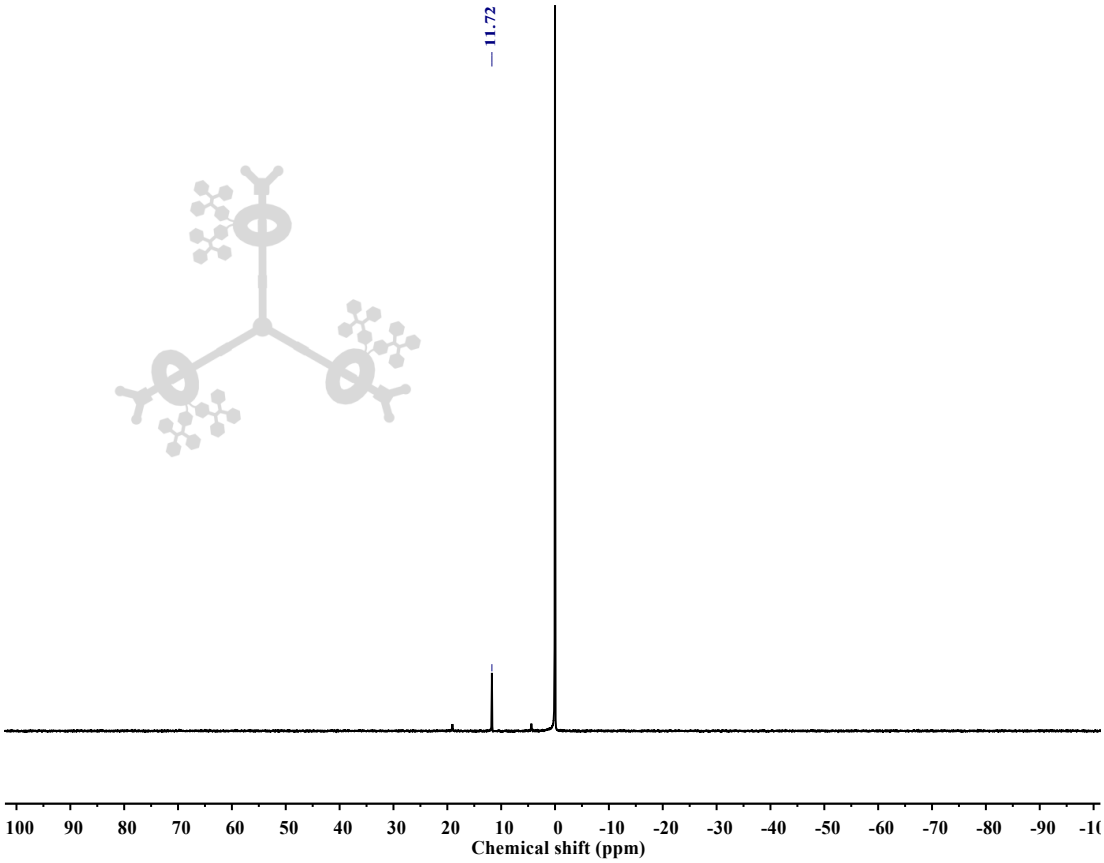

Figure S11. ^{31}P NMR spectrum (CD_2Cl_2, 298 K, 162 MHz) of **TPE-G1**.

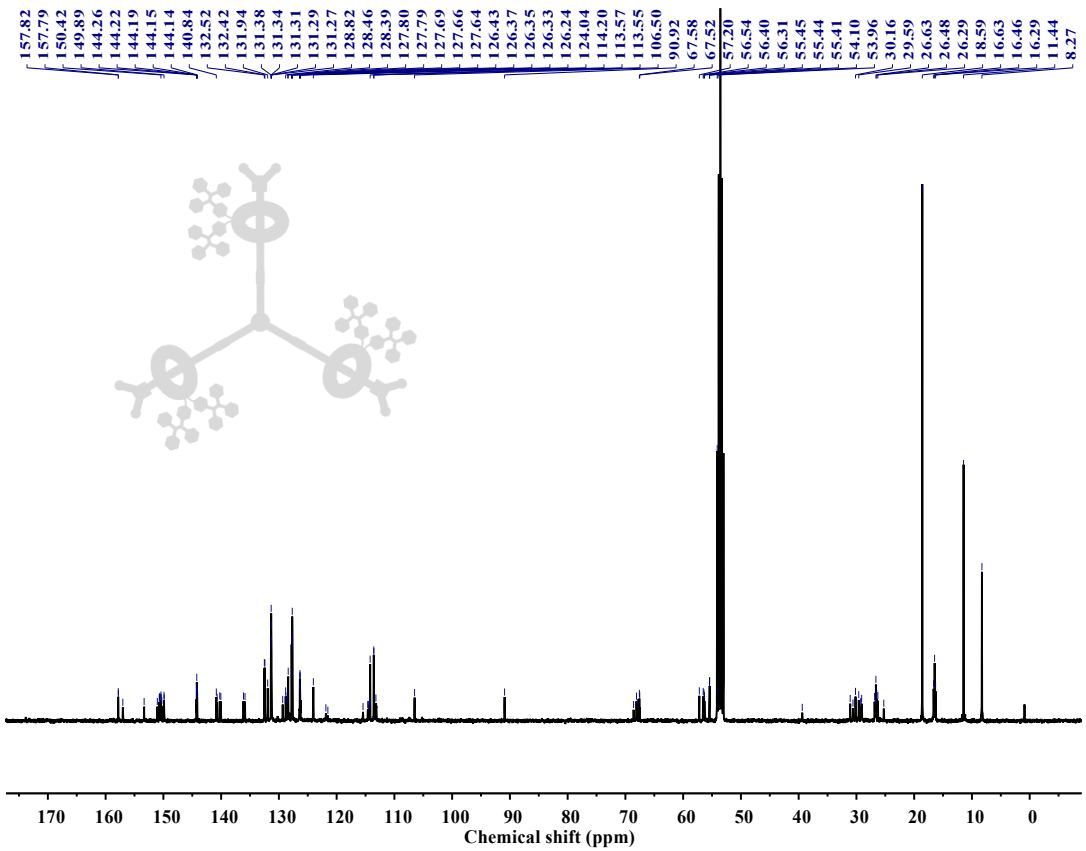

Figure S12. ^{13}C NMR spectrum (CD_2Cl_2, 298 K, 101 MHz) of **TPE-G1**.

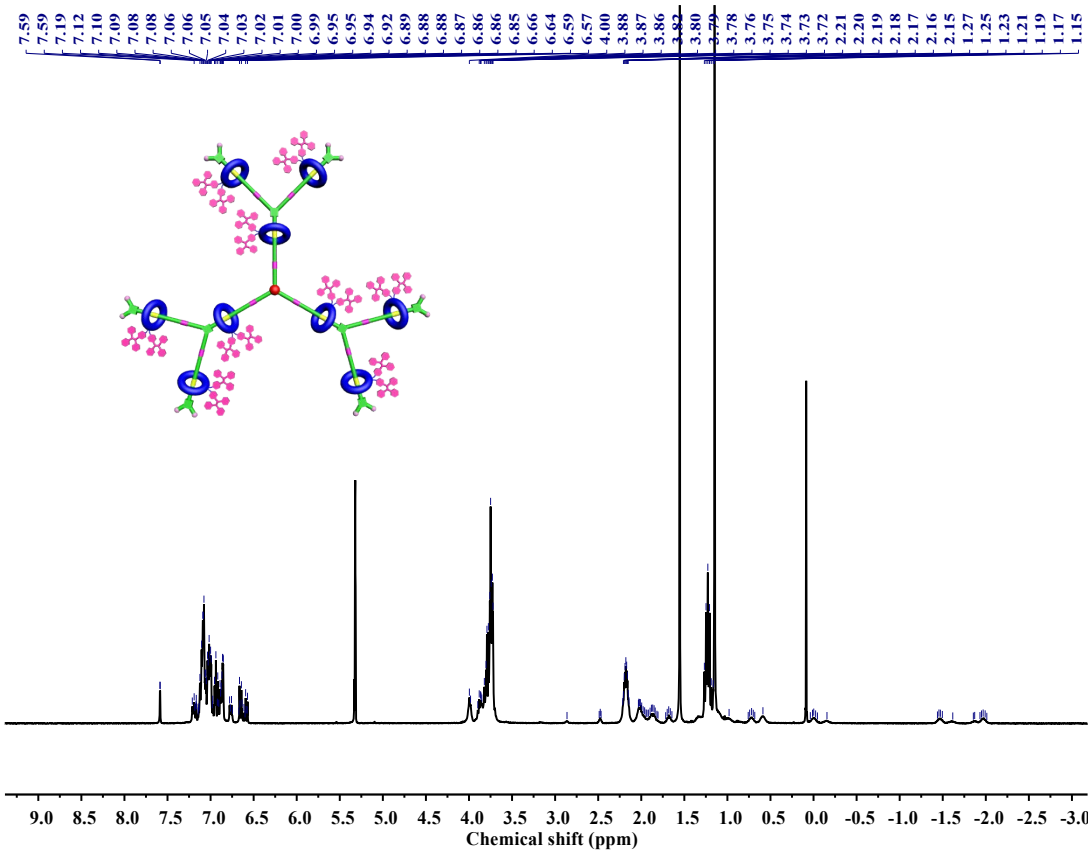

Figure S13. ^{1}H NMR spectrum (CD_2Cl_2, 298 K, 400 MHz) of **TPE-G2**.

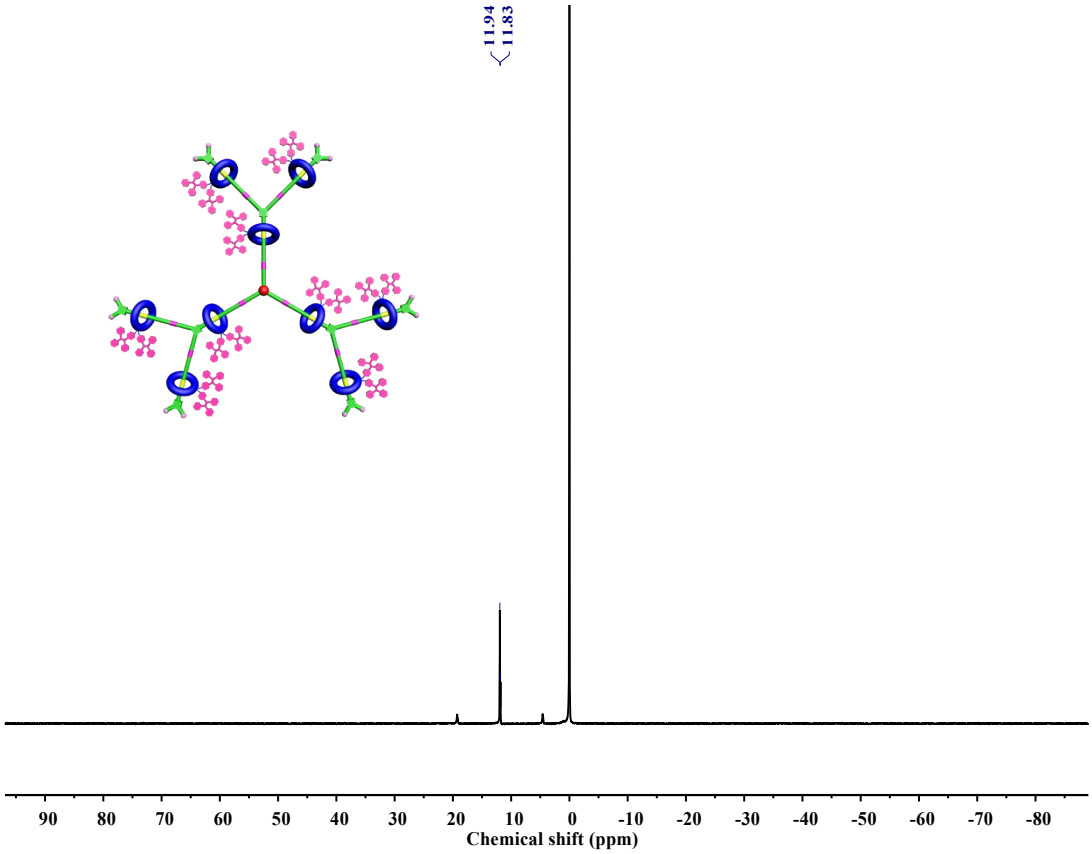

Figure S14. ^{31}P NMR spectrum (CD_2Cl_2, 298 K, 162 MHz) of **TPE-G2**.

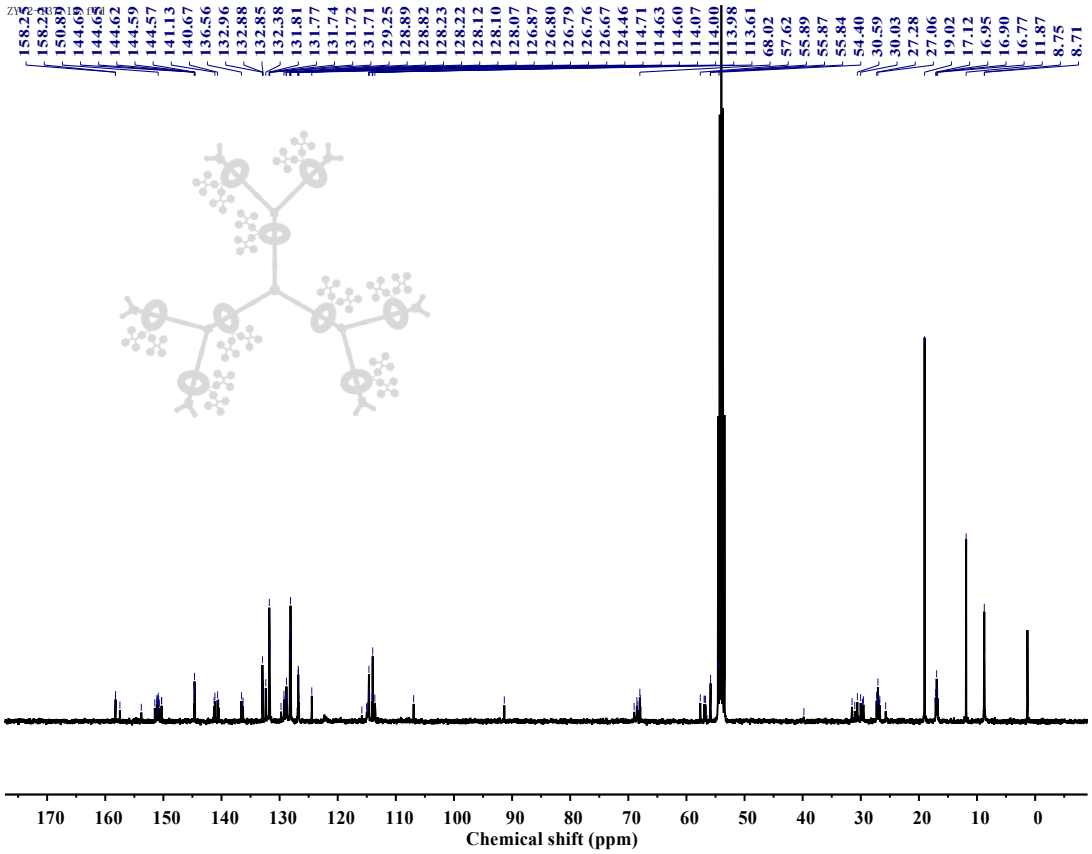

Figure S15. ^{13}C NMR spectrum (CD_2Cl_2, 298 K, 101 MHz) of **TPE-G2**.

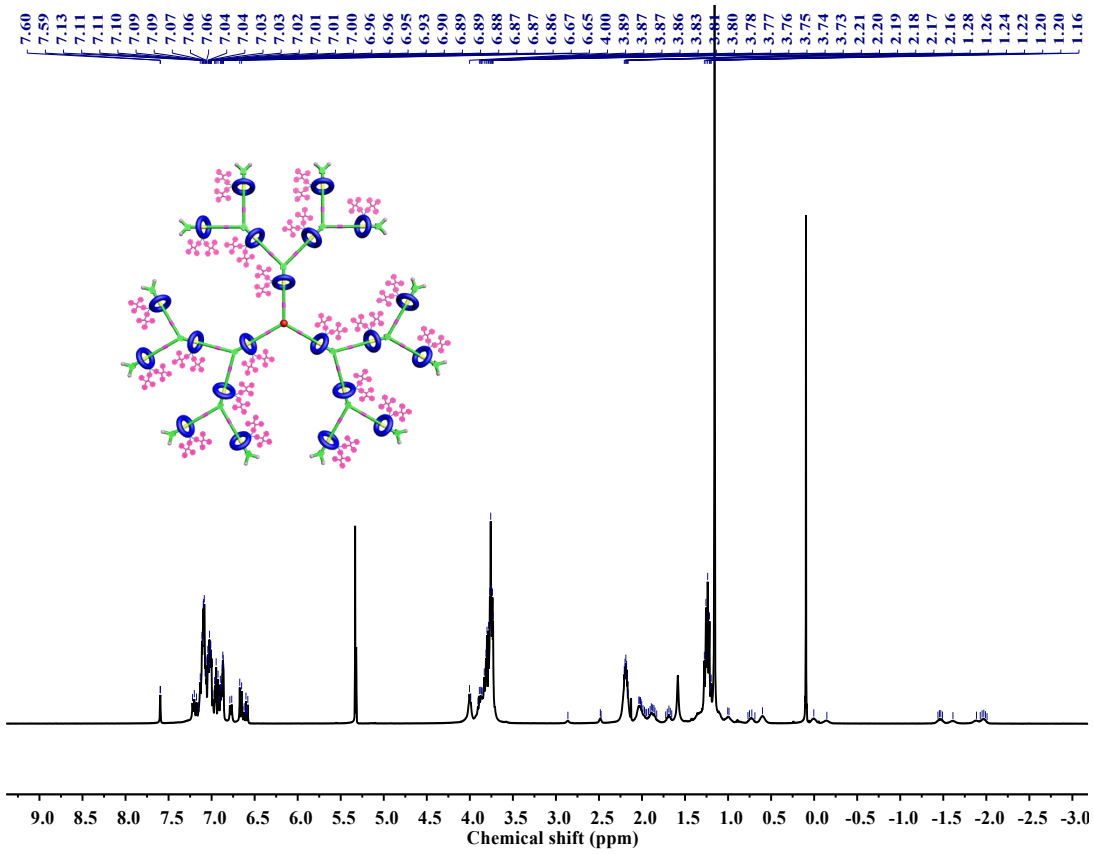

Figure S16. ^{1}H NMR spectrum (CD_2Cl_2, 298 K, 400 MHz) of **TPE-G3**.

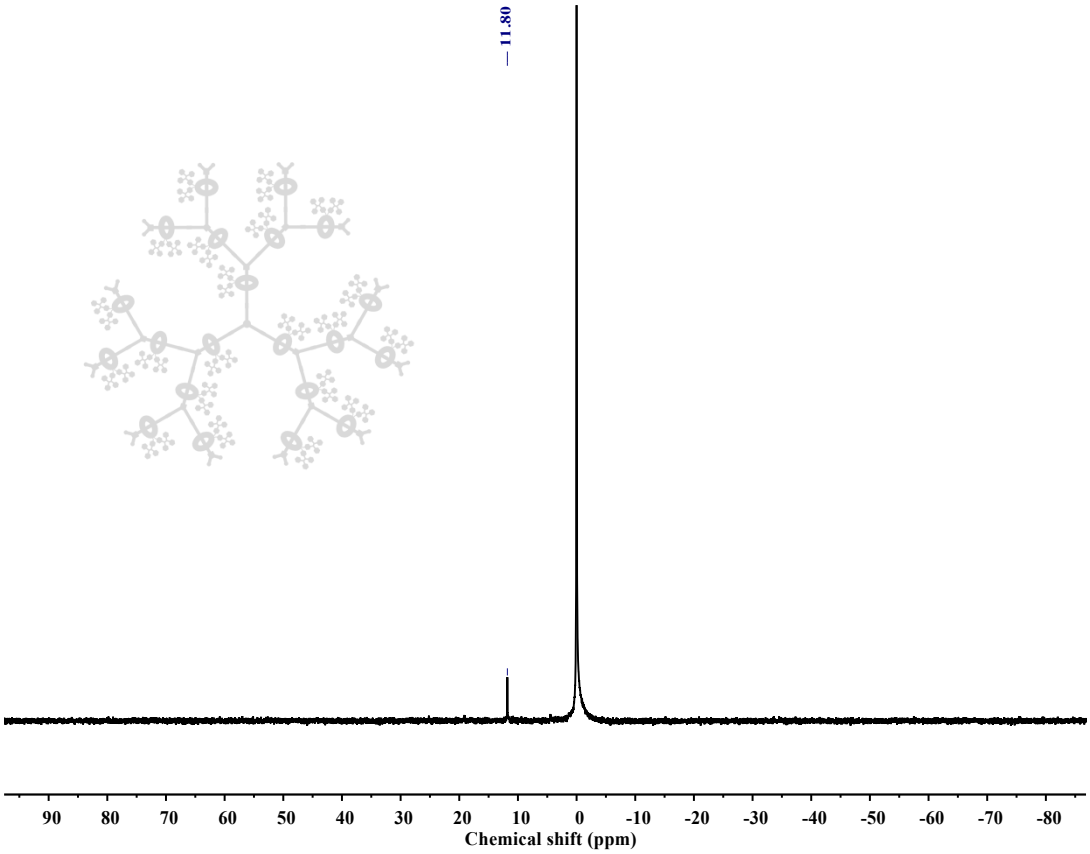

Figure S17. ^{31}P NMR spectrum (CD_2Cl_2, 298 K, 162 MHz) of **TPE-G3**.

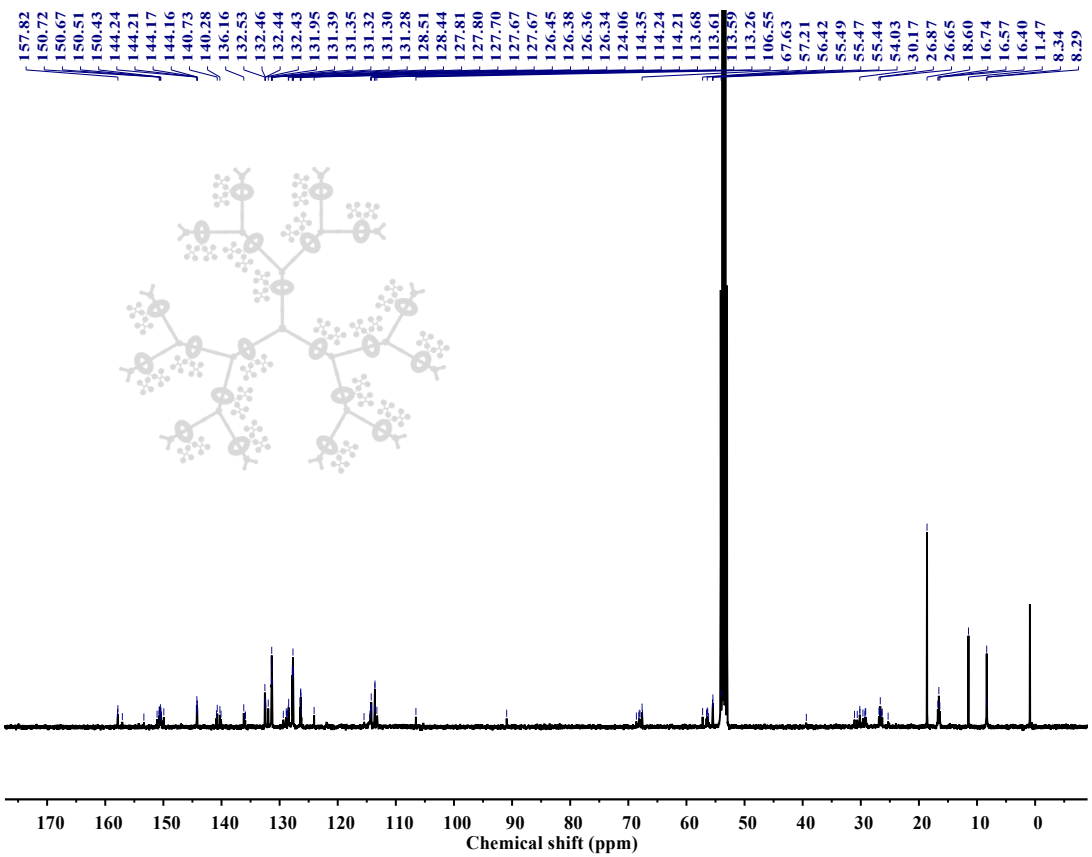

Figure S18. ^{13}C NMR spectrum (CD_2Cl_2, 298 K, 101 MHz) of **TPE-G3**.

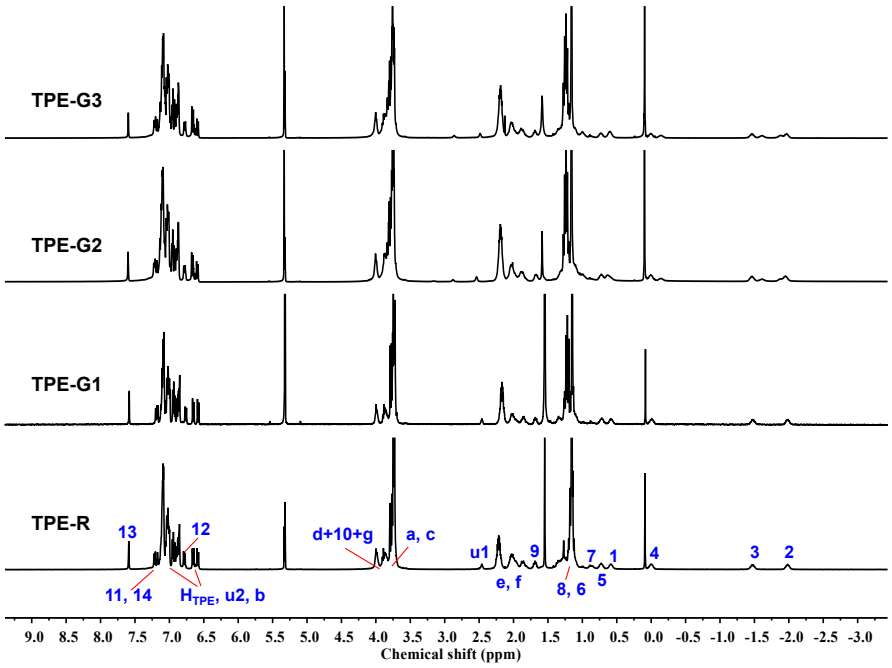

Figure S19. ^{1}H NMR spectra (CD_2Cl_2, 298 K, 400 MHz) of **TPE-Gn** (n = 1, 2, 3) and [2]rotaxane **TPE-R**. As revealed by the ^{1}H NMR spectra of **TPE-Gn** (n = 1, 2, 3), the signals of protons attributed to the rotaxane units, especially ones below 0.0 ppm that were ascribed to the encapsulated methylene protons ($H_{2\text{-}3}$), remained. This observation suggested that the rotaxane units kept intact during the dendrimer growth process.

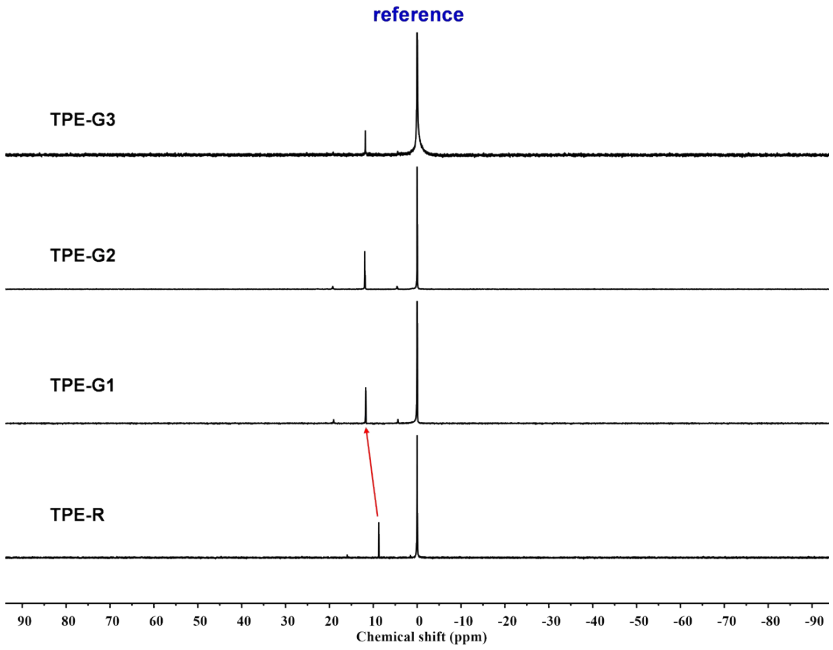

Figure S20. ^{31}P NMR spectra (CD_2Cl_2, 298 K, 162 MHz) of **TPE-Gn** (n = 1, 2, 3) and [2]rotaxane **TPE-R**. For all AIE-active rotaxane dendrimers **TPE-Gn** (n = 1, 2, 3), sharp peaks were observed in their ^{31}P NMR spectra, which clearly indicated the formation of highly symmetric dendritic skeletons.

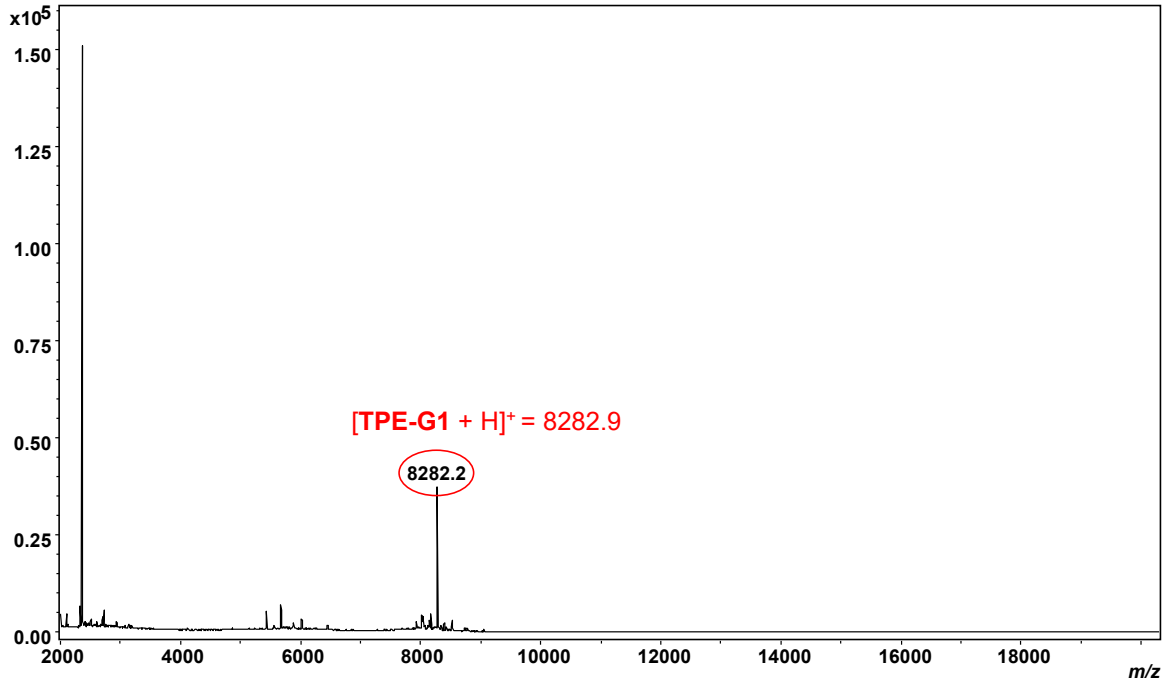

Figure S21. LRMS (MALDI-TOF-MS) spectrum of **TPE-G1**. The peak of *m/z* = 8282.2 was found, which agreed well with the theoretical value of [**TPE-G1** + H]$^+$ ion (*m/z* = 8282.9).

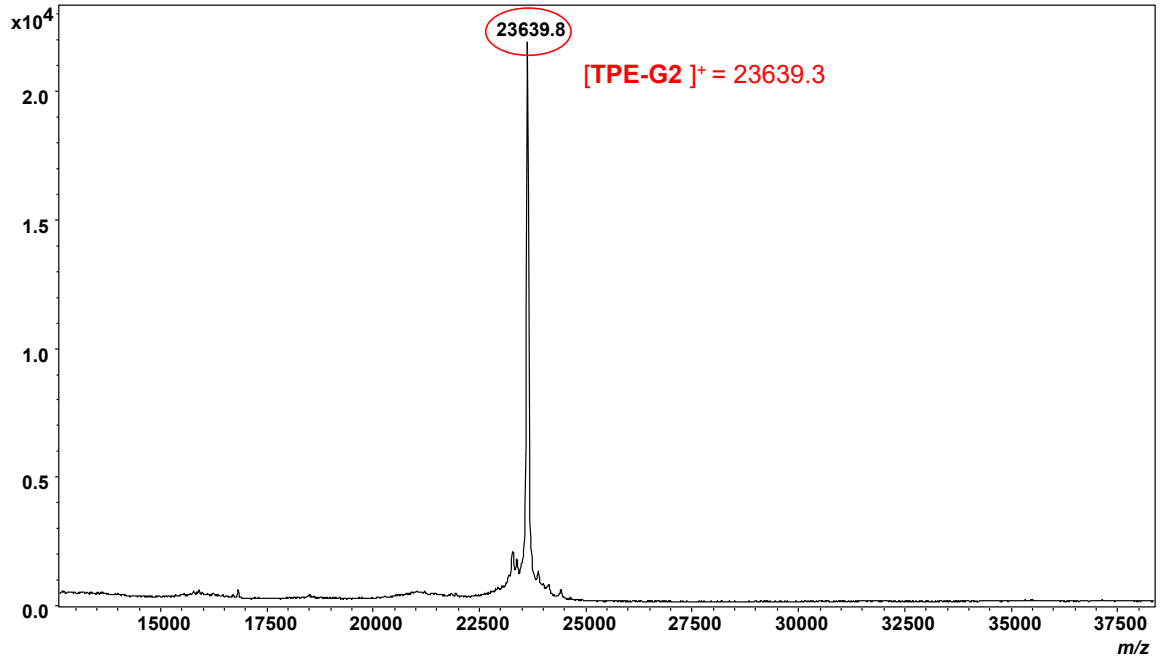

Figure S22. LRMS (MALDI-TOF-MS) spectrum of **TPE-G2**. The peak of *m/z* = 23639.8 was found, which agreed well with the theoretical value of [**TPE-G2**]$^+$ ion (*m/z* = 23639.3).

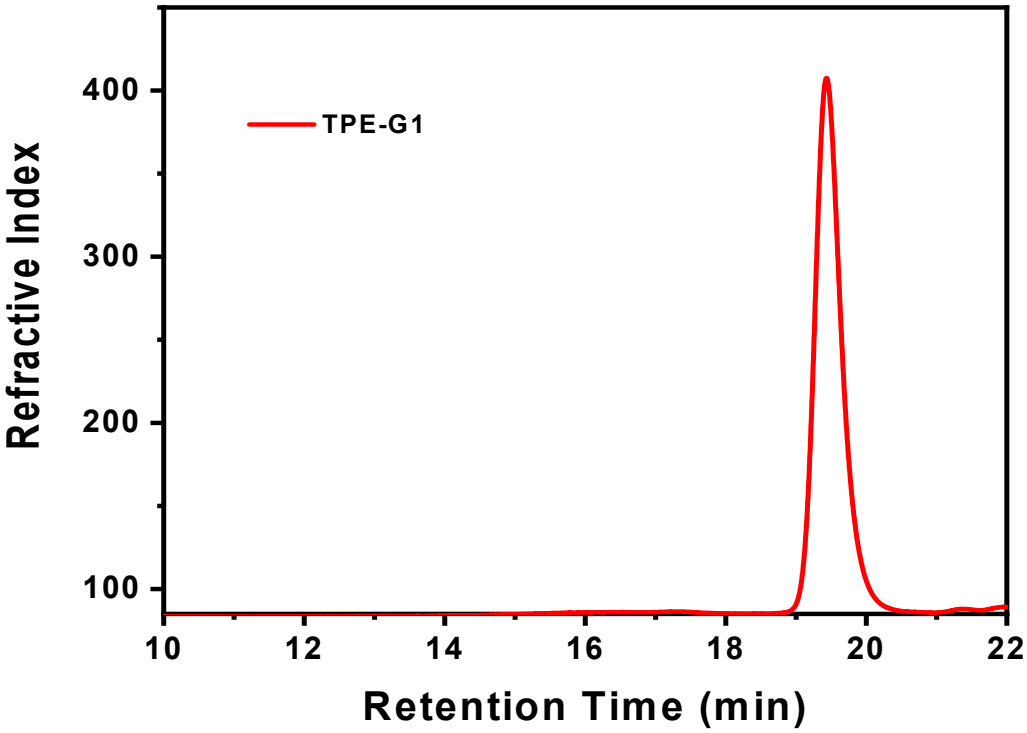

Figure S23. GPC curve of rotaxane dendrimer **TPE-G1**, PDI = 1.02, M_n = 7825.

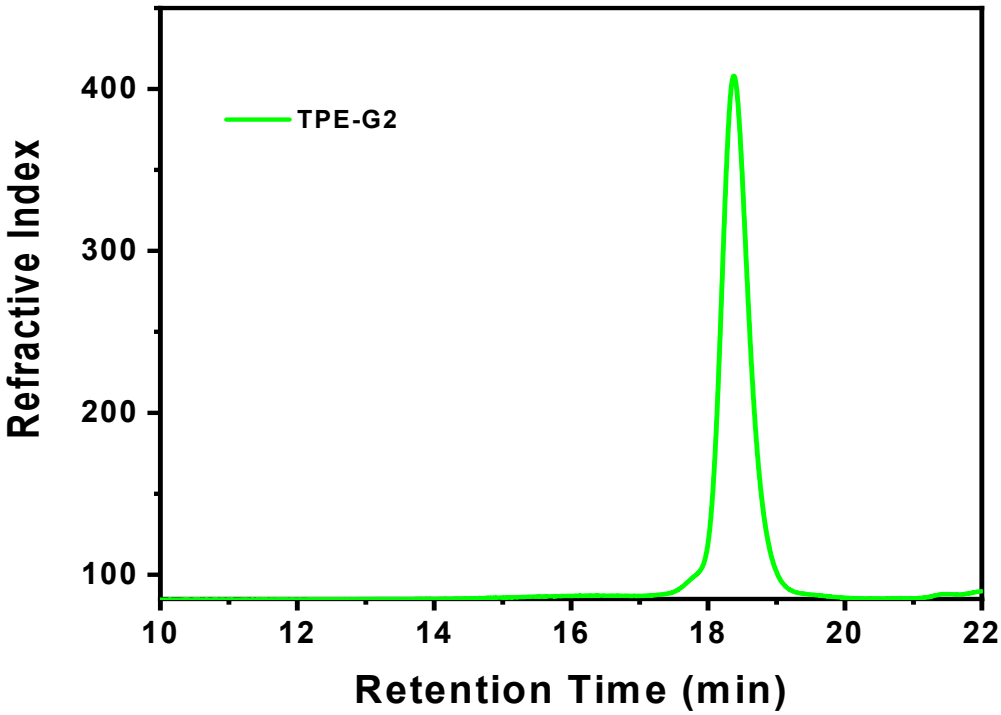

Figure S24. GPC curve of rotaxane dendrimer **TPE-G2**, PDI = 1.02, M_n = 21826.

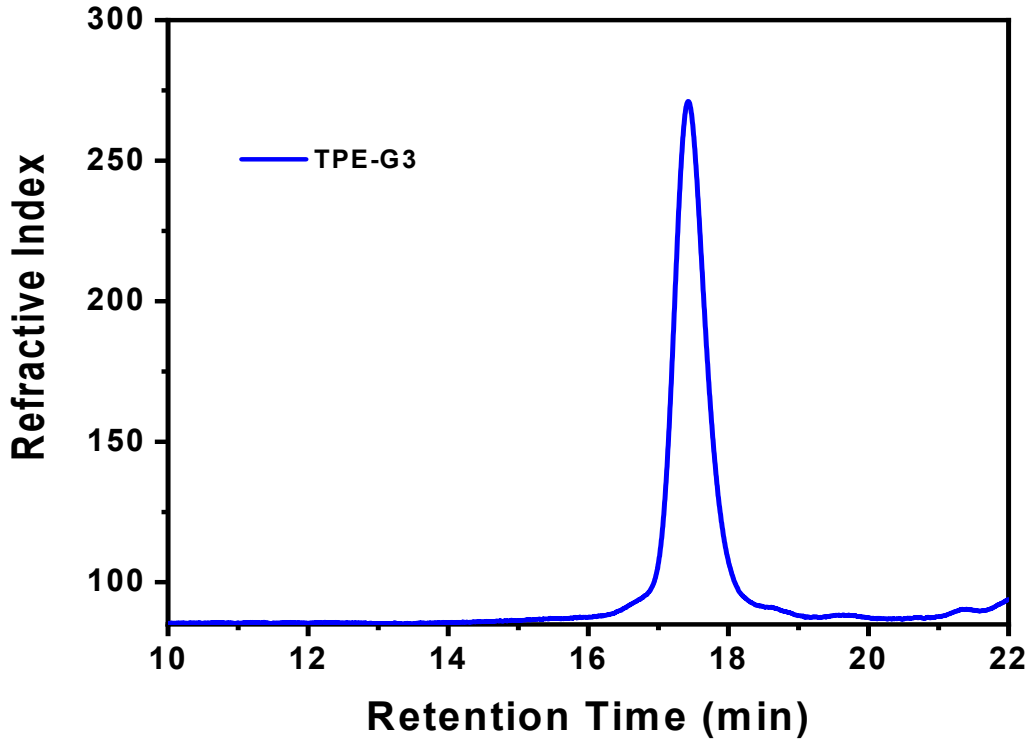

Figure S25. GPC curve of rotaxane dendrimer **TPE-G3**, PDI = 1.05, M_n = 41439.

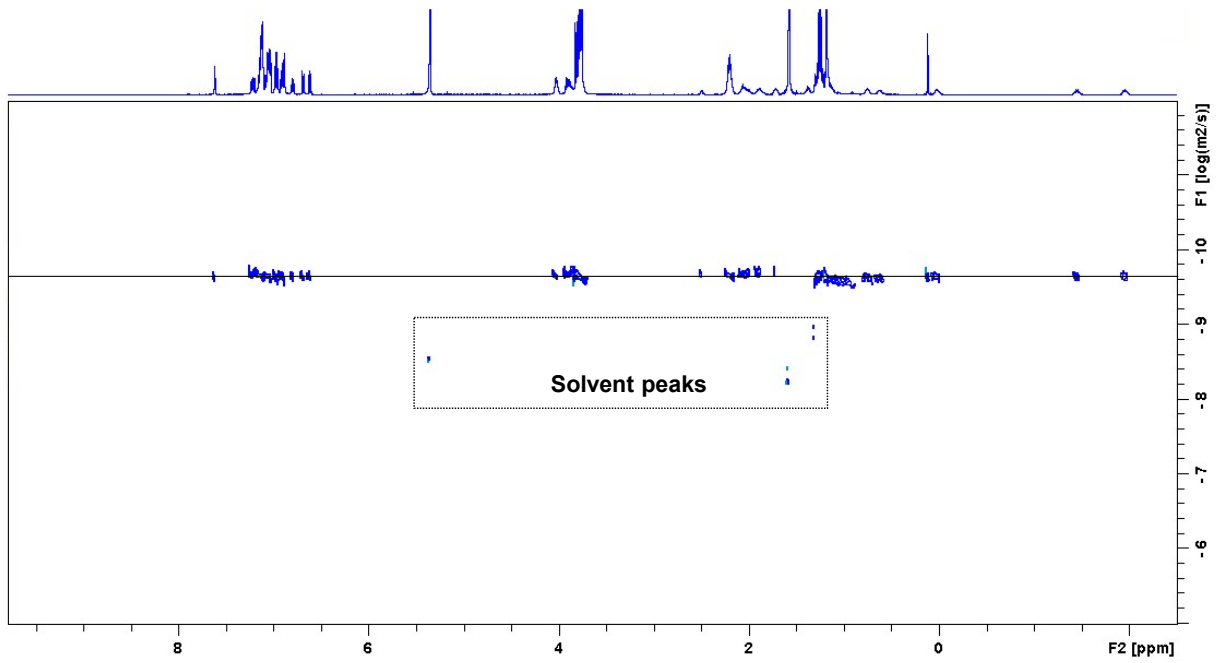

Figure S26. 2-D DOSY spectrum (CD_2Cl_2, 298 K, 500 MHz) of **TPE-G1**, the diffusion coefficient $D = (2.19 \pm 0.10) \times 10^{-10}$ m^2 s^{-1}, D_T = 4.7 nm.

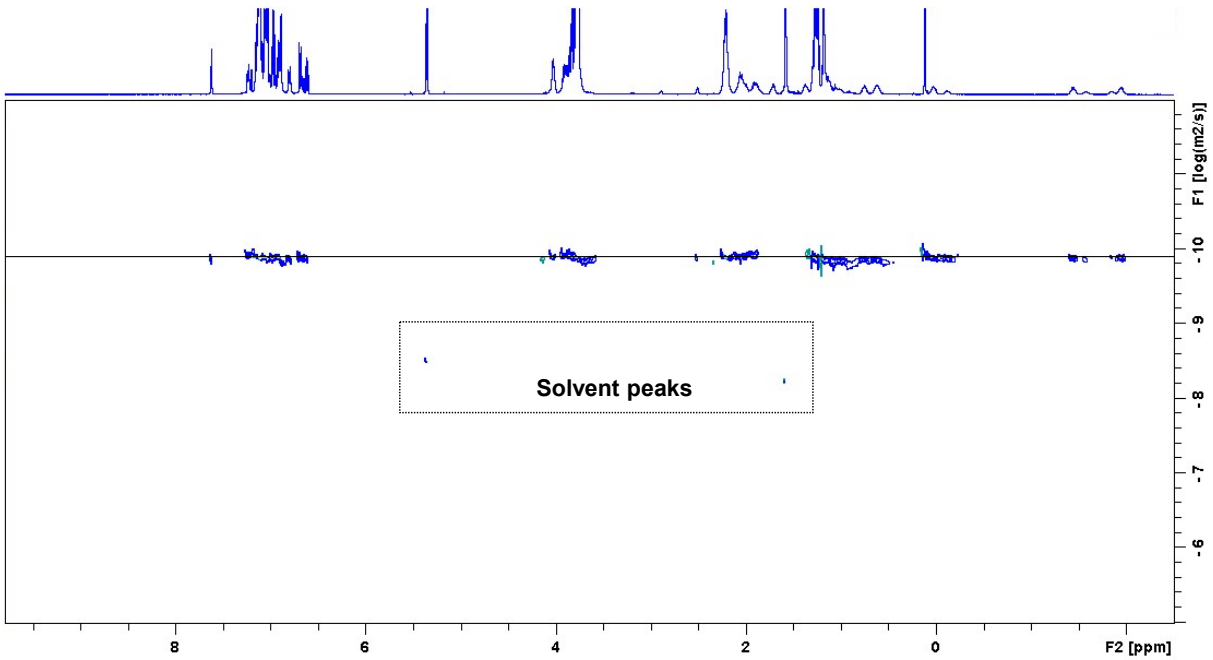

Figure S27. 2-D DOSY spectrum (CD_2Cl_2, 298 K, 500 MHz) of **TPE-G2**, the diffusion coefficient $D = (1.32 \pm 0.11) \times 10^{-10}$ m^2 s^{-1}, $D_T = 7.8$ nm.

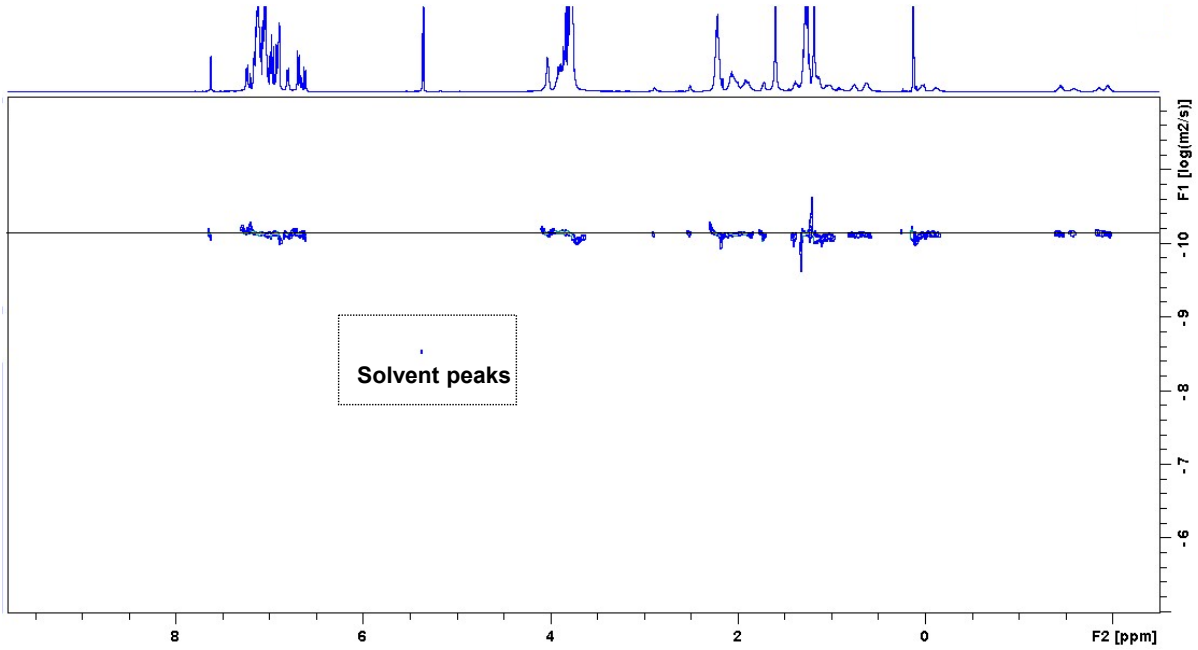

Figure S28. 2-D DOSY spectrum (CD_2Cl_2, 298 K, 500 MHz) of **TPE-G3**, the diffusion coefficient $D = (7.41 \pm 0.13) \times 10^{-11}$ m^2 s^{-1}, $D_T = 13.9$ nm.

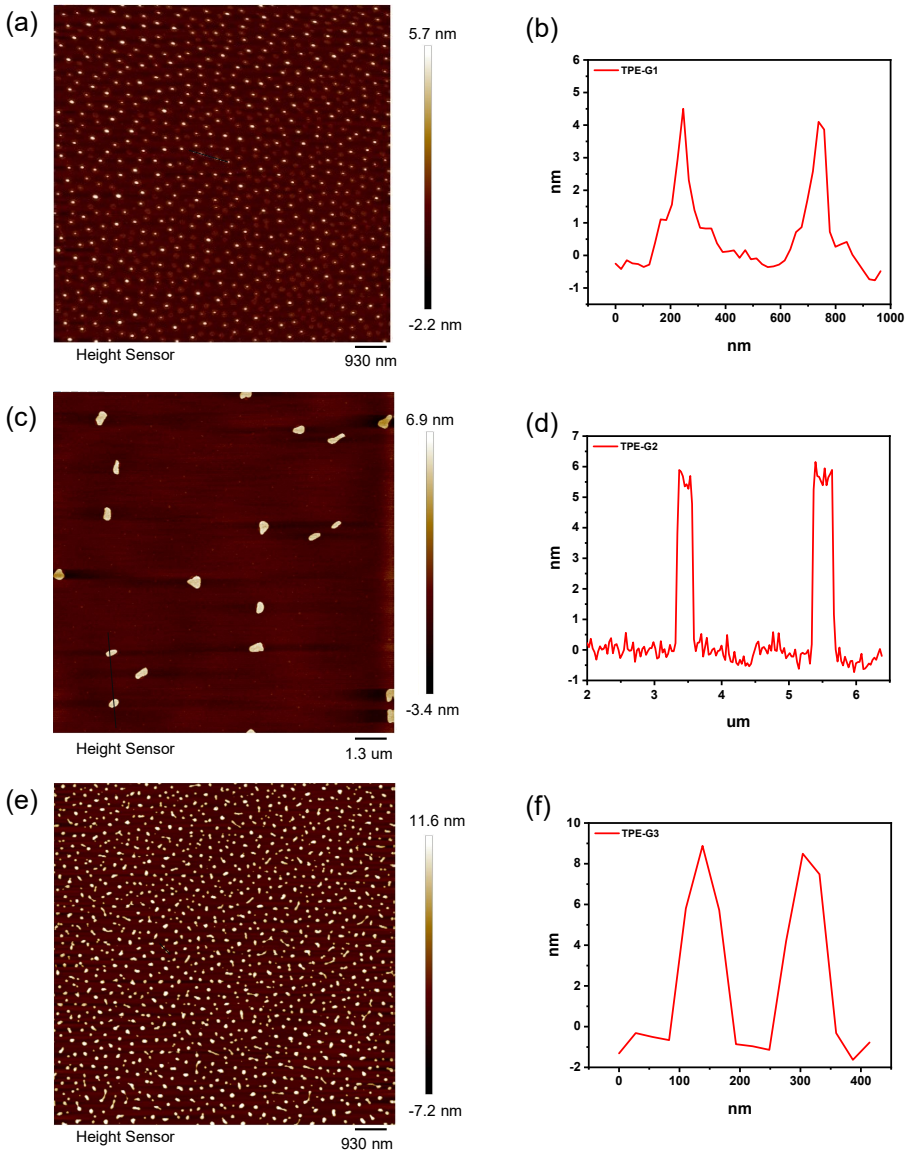

Figure S29. AFM images of the rotaxane-branched dendrimers. (a)**TPE-G1**; (b) height range of **TPE-G1** is 4.1 ± 0.2 nm; (c) **TPE-G2**; (d) height range of **TPE-G2** is 5.9 ± 0.1 nm; (e) **TPE-G3**; (f) height range of **TPE-G3** is 8.8 ± 0.3 nm.

Section D. Anion-induced switching behavior of [2]rotaxane TPE-R and rotaxane dendrimers TPE-Gn (n = 1, 2, 3)

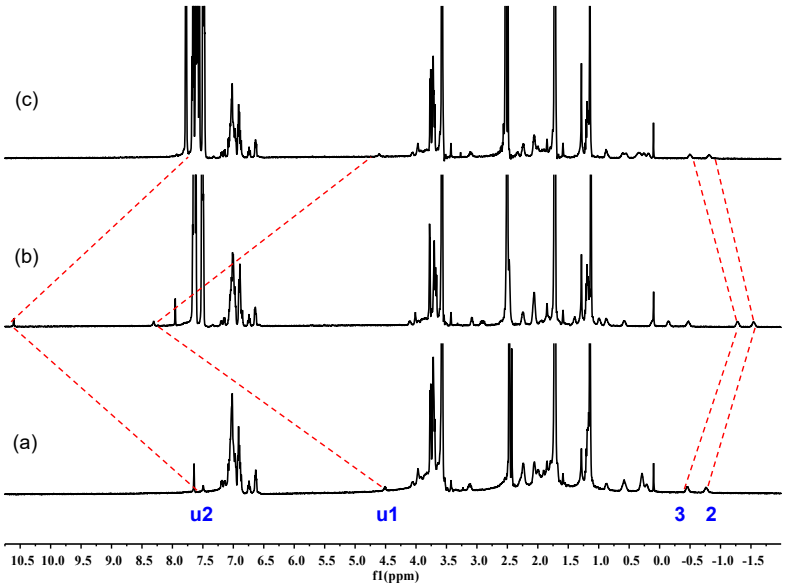

Figure S30. Stacked ^{1}H NMR spectra (THF-d_8, 298 K, 500 MHz) of anion-induced switching behavior of [2]rotaxane **TPE-R**. a) **TPE-R**; b) the mixture of **TPE-R** and 5 eq. CF_3COO^- (for each rotaxane unit); c) the mixture obtained after adding 7 eq. Na^+ (for each rotaxane unit) to the solution in b).

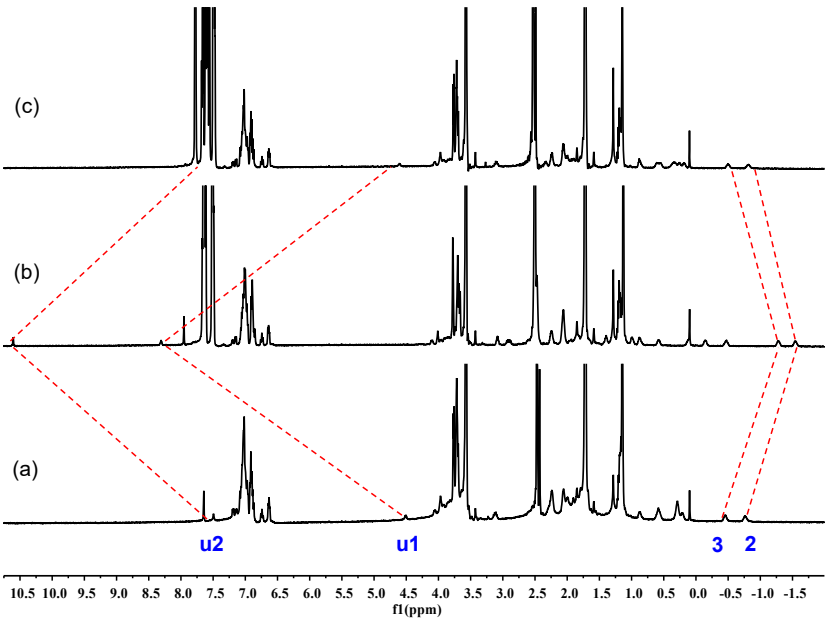

Figure S31. Stacked ^{1}H NMR spectra (THF-d_8, 298 K, 500 MHz) of anion-induced switching behavior of rotaxane dendrimer **TPE-G1**. a) **TPE-G1**; b) the mixture of **TPE-G1** and 5 eq. CF_3COO^- (for each rotaxane unit); c) the mixture obtained after adding 7 eq. Na^+ (for each rotaxane unit) to the solution in b).

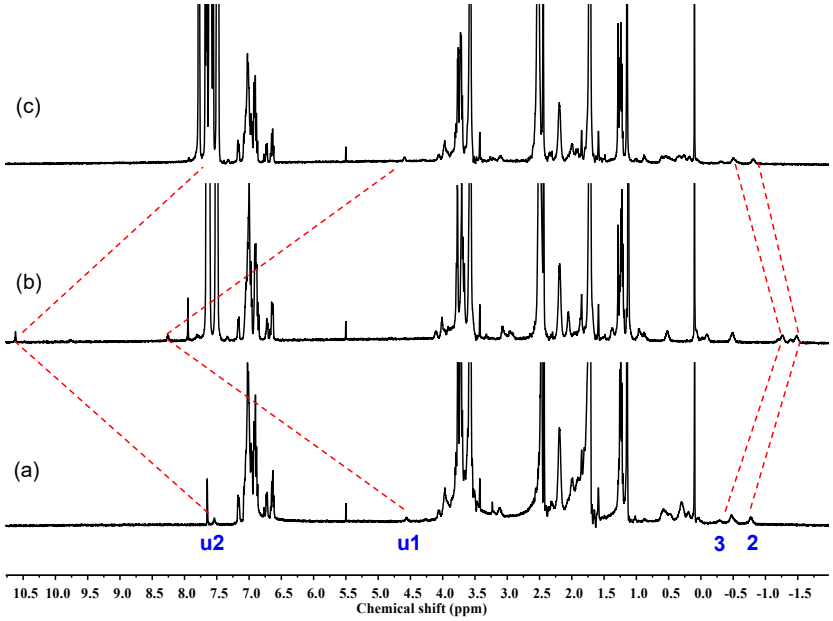

Figure S32. Stacked ^{1}H NMR spectra (THF-d_8, 298 K, 500 MHz) of anion-induced switching behavior of rotaxane dendrimer **TPE-G2**. a) **TPE-G2**; b) the mixture of **TPE-G2** and 5 eq. CF_3COO^- (for each rotaxane unit); c) the mixture obtained after adding 7 eq. Na^+ (for each rotaxane unit) to the solution in b).

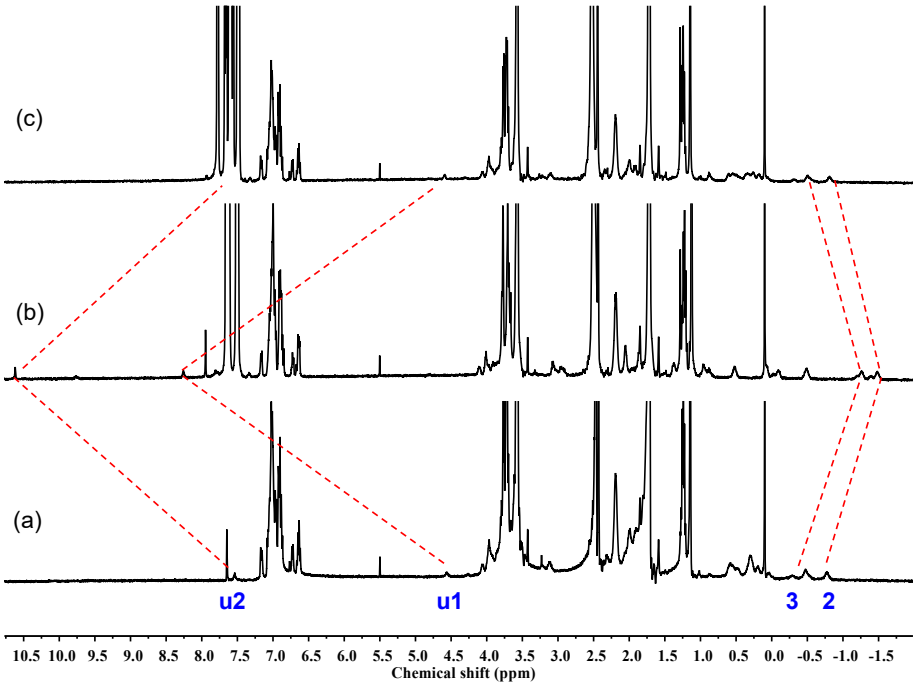

Figure S33. Stacked ^{1}H NMR spectra (THF-d_8, 298 K, 500 MHz) of anion-induced switching behavior of rotaxane dendrimer **TPE-G3**. a) **TPE-G3**; b) the mixture of **TPE-G3** and 5 eq. CF_3COO^- (for each rotaxane unit); c) the mixture obtained after adding 7 eq. Na^+ (for each rotaxane unit) to the solution in b).

Section E. Aggregation-induced emission behaviors of rotaxane dendrimers TPE-Gn (n = 1, 2, 3)

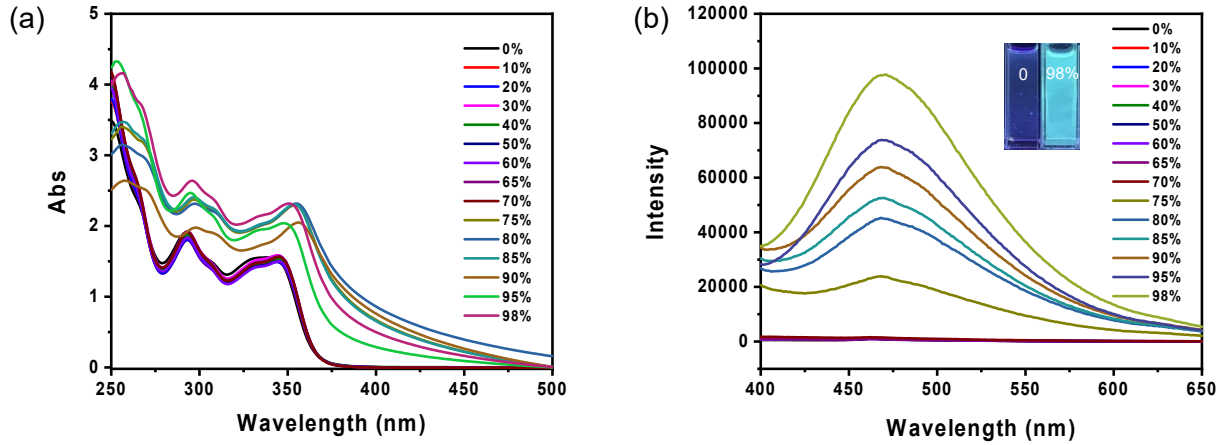

Figure S34. (a) UV-vis spectra and (b) Fluorescence spectra (λ_{ex} = 345 nm) of rotaxane dendrimer **TPE-G1** ([TPE units] = 50 μM) in DCM/ACN with different ACN fractions. *Inset*: photographs in DCM/ACN with 0 (*left*) and 98% (*right*) ACN fractions taken under UV illumination (λ_{ex} = 365 nm).

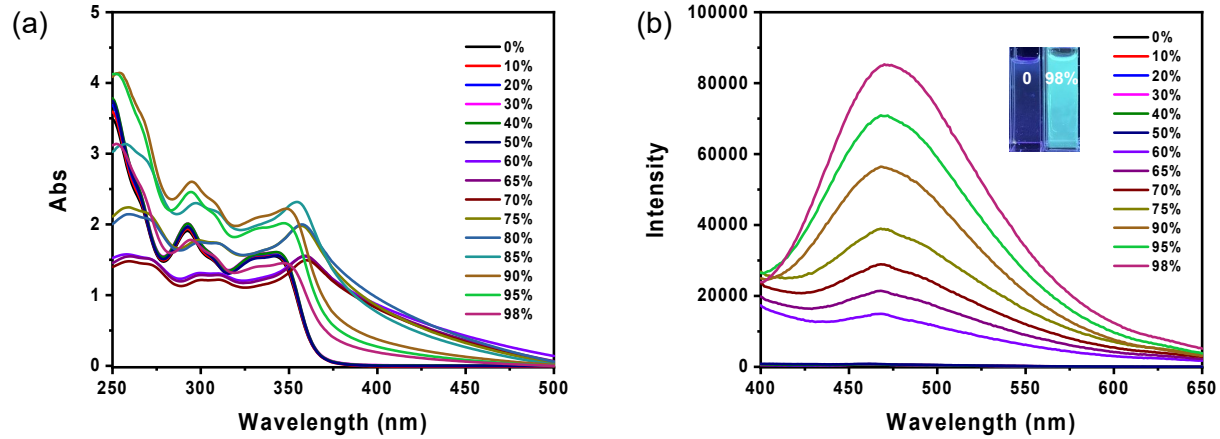

Figure S35. (a) UV-vis spectra and (b) Fluorescence spectra (λ_{ex} = 345 nm) of rotaxane dendrimer **TPE-G2** ([TPE units] = 50 μM) in DCM/ACN with different ACN fractions. *Inset*: photographs in DCM/ACN with 0 (*left*) and 98% (*right*) ACN fractions taken under UV illumination (λ_{ex} = 365 nm).

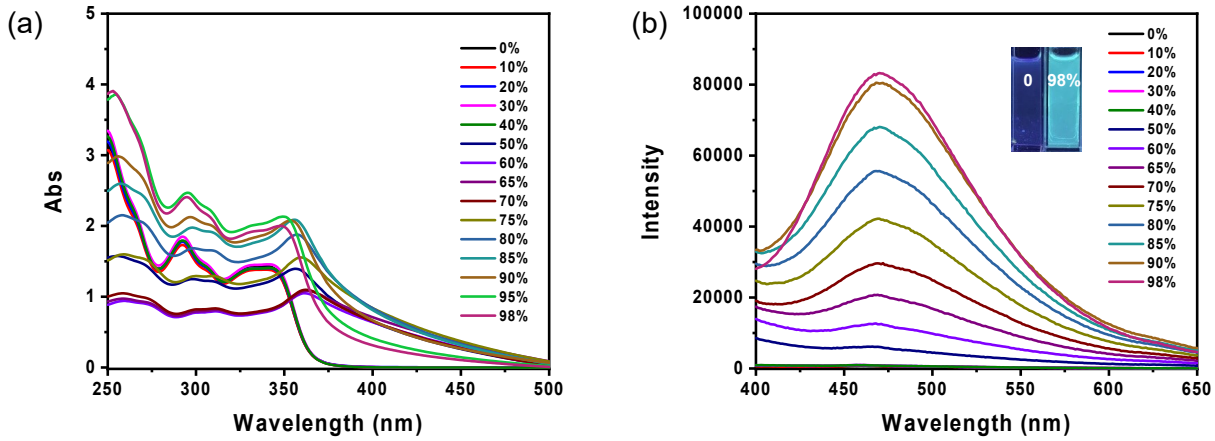

Figure S36. (a) UV-vis spectra and (b) Fluorescence spectra (λ_{ex} = 345 nm) of rotaxane dendrimer **TPE-G3** ([TPE units] = 50 μM) in DCM/ACN with different ACN fractions. *Inset*: photographs in DCM/ACN with 0 (*left*) and 98% (*right*) ACN fractions taken under UV illumination (λ_{ex} = 365 nm).

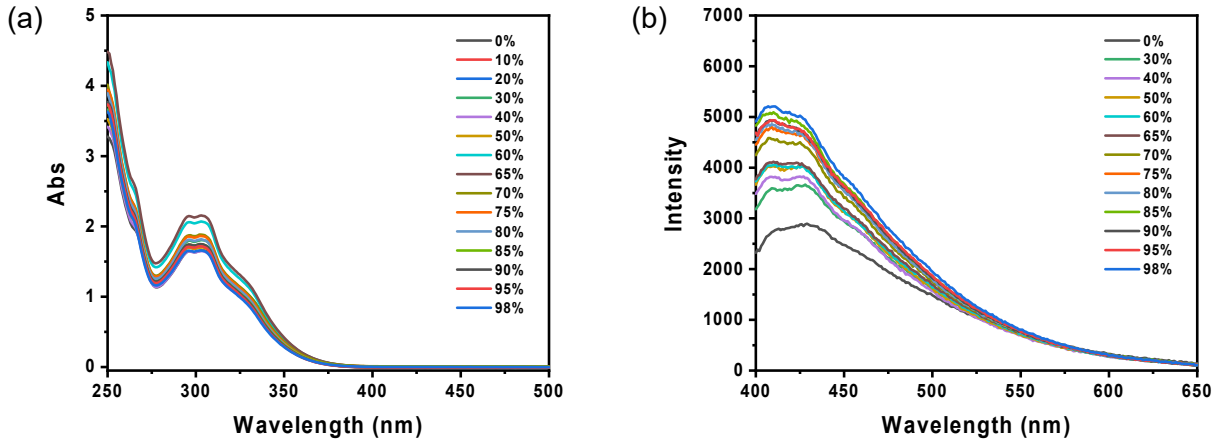

Figure S37. (a) UV-vis spectra and (b) Fluorescence spectra (λ_{ex} = 345 nm) of [2]rotaxane **TPE-R** ([TPE units] = 50 μM) in DCM/ACN with different ACN fractions. *Inset*: photographs in DCM/ACN with 0 (*left*) and 98% (*right*) ACN fractions taken under UV illumination (λ_{ex} = 365 nm).

Quantum yield measurements

Table S1. The photophysical parameters of the rotaxane dendrimers **TPE-Gn** (n = 1, 2, 3) and [2]rotaxane **TPE-R** ([TPE units] = 50 μM in DCM/ACN with 98% ACN fractions, measured at 25 °C).

Compound	λ_{em} (nm)	Φ_F (%)[a]
TPE-R	430	*
TPE-G1	480	0.2
TPE-G2	480	1.9
TPE-G3	480	1.4

[a]The absolute fluorescence quantum yields were measured in solution using a commercial fluorometer with integrating sphere.

* Too low to be measured.

Section F. Artificial light-harvesting systems TPE-Gn-ESY (n = 1, 2, 3) based on rotaxane dendrimers

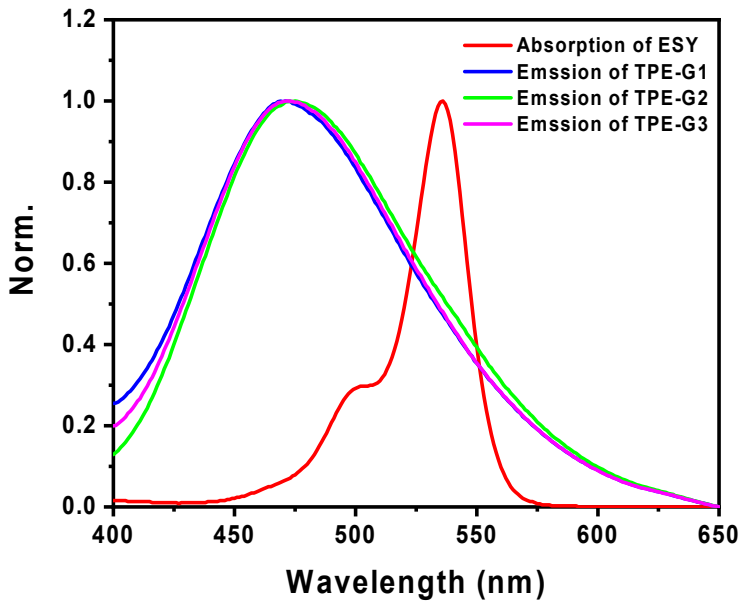

Figure S38. Normalized absorption of ESY and fluorescence spectra of **TPE-Gn** (n = 1, 2, 3) (λ_{ex} = 345 nm) in DCM/ACN (v/v = 2/98).

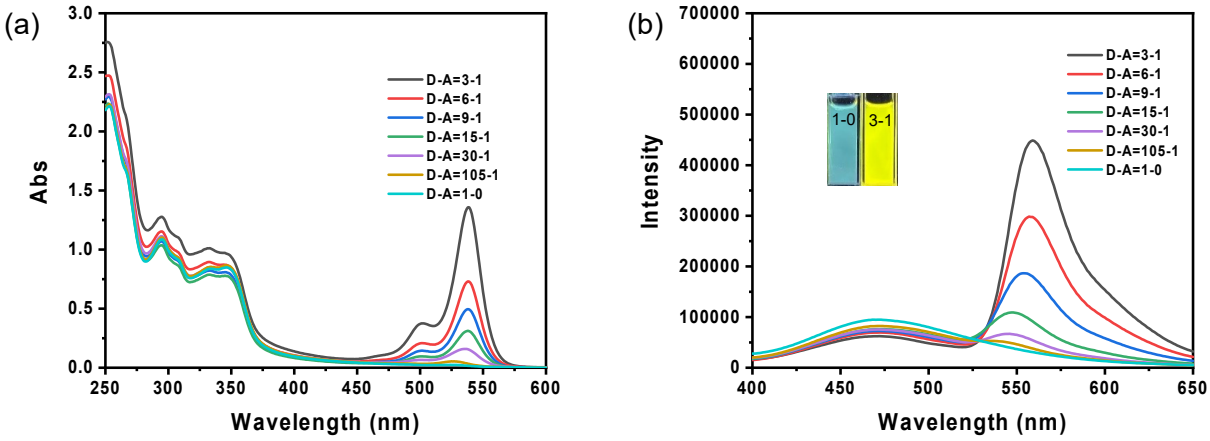

Figure S39. (a) Absorption and (b) fluorescence spectra of **TPE-G1-ESY** system ([TPE units] = 50 μM, λ_{ex} = 345 nm) in DCM/ACN (v/v = 2/98). *Inset*: photographs in D/A = 1/0 (left), 3/1 (right) taken under UV illumination (λ_{ex} = 365 nm). Donor (D) = TPE units, Acceptor (A) = eosin Y.

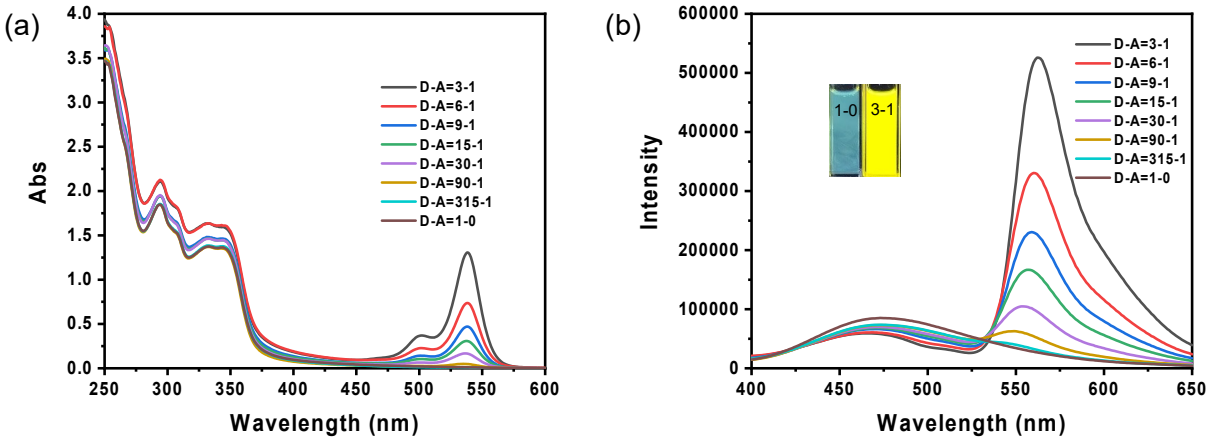

Figure S40. (a) Absorption and (b) fluorescence spectra of **TPE-G2-ESY** system ([TPE units] = 50 μM, λ_{ex} = 345 nm) in DCM/ACN (v/v = 2/98). *Inset*: photographs in D/A = 1/0 (left), 3/1 (right) taken under UV illumination (λ_{ex} = 365 nm). Donor (D) = TPE units, Acceptor (A) = eosin Y.

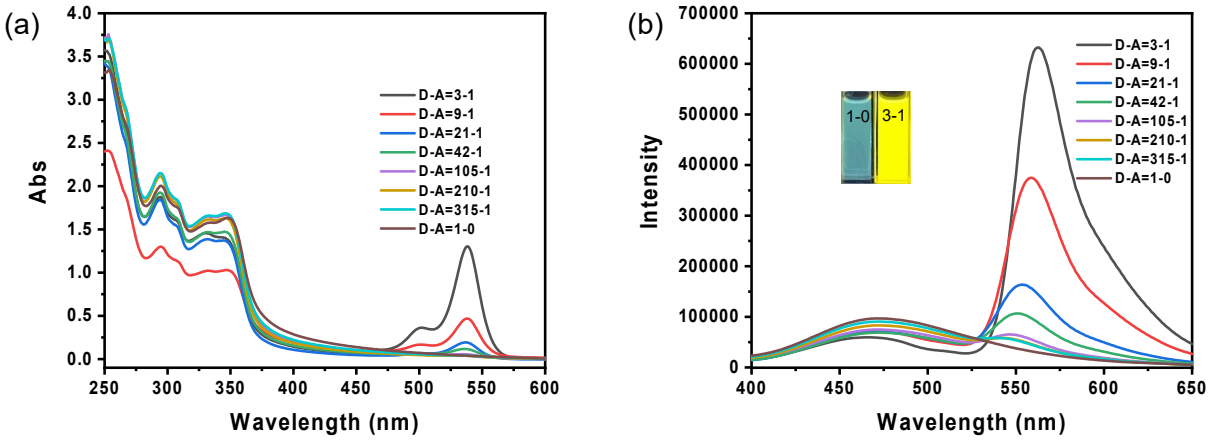

Figure S41. (a) Absorption and (b) fluorescence spectra of **TPE-G3-ESY** system ([TPE units] = 50 μM, λ_{ex} = 345 nm) in DCM/ACN (v/v = 2/98). *Inset*: photographs in D/A = 1/0 (left), 3/1 (right) taken under UV illumination (λ_{ex} = 365 nm). Donor (D) = TPE units, Acceptor (A) = eosin Y.

Energy-transfer efficiency

Energy-transfer efficiency, Φ_{ET}, the fraction of the absorbed energy that is transferred to the acceptor is experimentally measured as a ratio of the fluorescence intensities of the donor in the absence and presence of the acceptor (I_D and I_{DA})[S3]. And it was calculated by the following equation:

$$\Phi ET = 1 - \frac{IDA}{ID}$$

Based on the above equation and the spectra presented in Figures S41-43, the energy-transfer efficiencies (Φ_{ET}) between donor and acceptor were calculated to be 34.5% (**TPE-G1-ESY**), 31.9% (**TPE-G2-ESY**), and 39.4% (**TPE-G3-ESY**), respectively.

The antenna effect (AE) under certain concentrations of donor and acceptor equals the ratio of the emission intensity of the acceptor upon excitation of the donor, $I_{AF\lambda(D)}$, to that of the direct excitation of the acceptor, $I_{AF\lambda(A)}$ [S3].

$$AE = \frac{IAF\lambda(DA, 345) - IAF\lambda(D, 345)}{IAF\lambda(A, 480)}$$

Based on the above equation and the spectra presented in Figures S44-46, the antenna effects (AE) were calculated to be 1.09 (**TPE-G1-ESY**), 1.11 (**TPE-G2-ESY**), and 1.79 (**TPE-G3-ESY**), respectively.

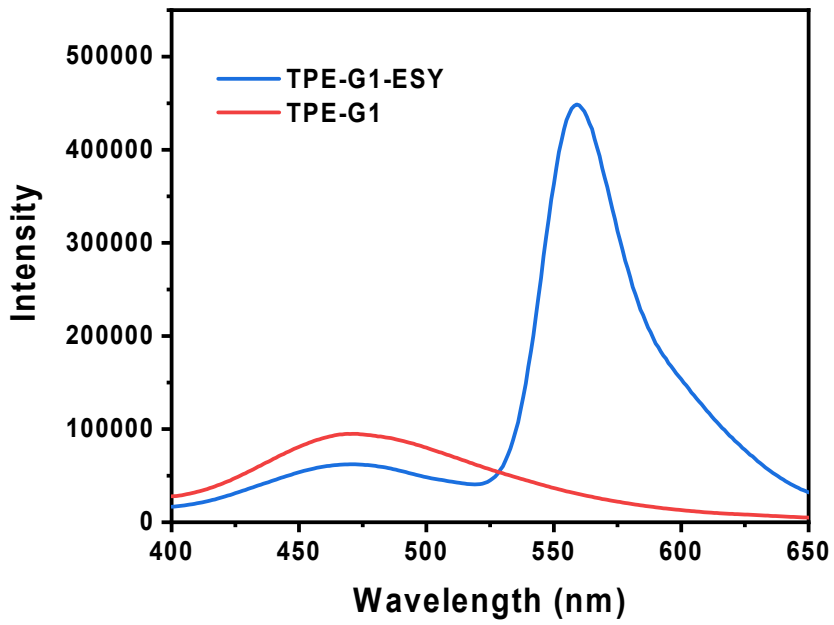

Figure S42. Fluorescence spectra of **TPE-G1** and **TPE-G1-ESY** system ([TPE units]/[ESY] = 3/1) in DCM/ACN (v/v = 2/98, excitation at 345 nm).

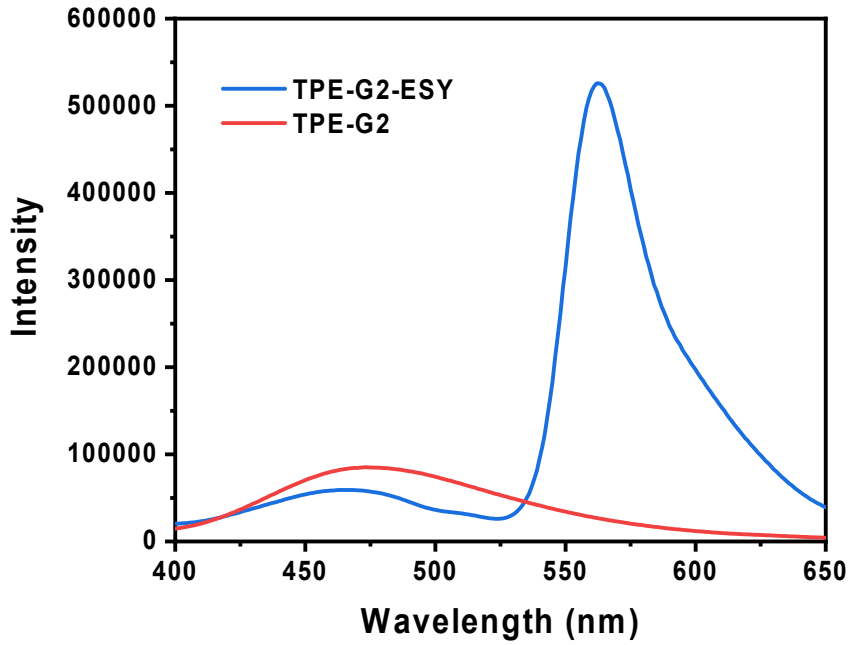

Figure S43. Fluorescence spectra of **TPE-G2** and **TPE-G2-ESY** system ([TPE units]/[ESY] = 3/1) in DCM/ACN (v/v = 2/98, excitation at 345 nm).

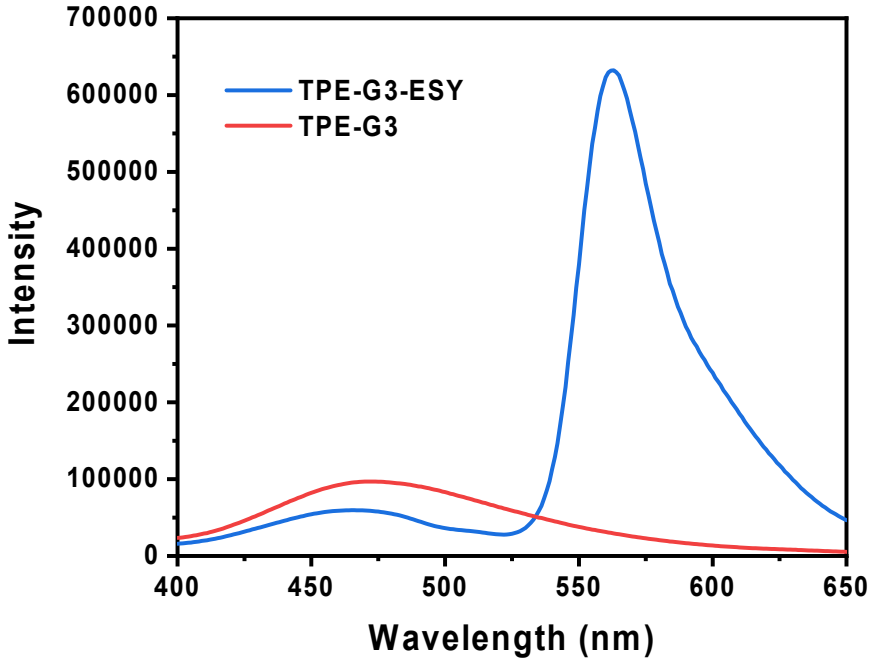

Figure S44. Fluorescence spectra of **TPE-G3** and **TPE-G3-ESY** system ([TPE units]/[ESY] = 3/1) in DCM/ACN (v/v = 2/98, excitation at 345 nm).

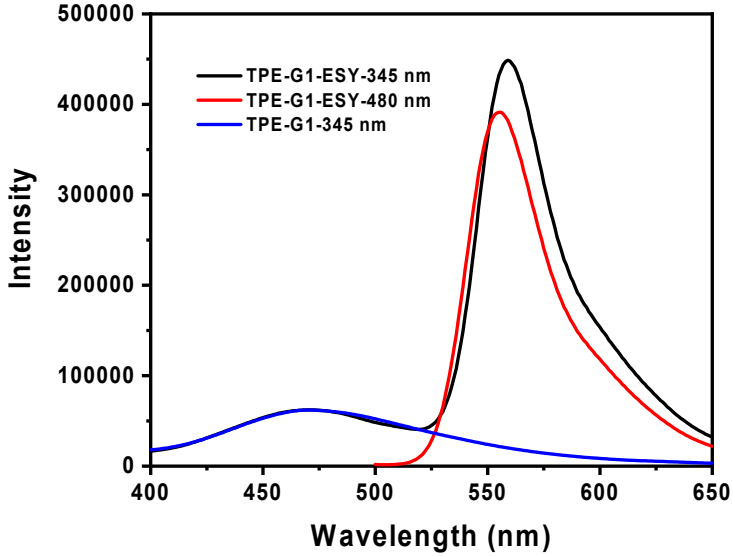

Figure S45. Fluorescence spectra of **TPE-G1-ESY** system ([TPE units]/[ESY] = 3/1) in DCM/ACN (v/v = 2/98) (black line, λ_{ex} = 345 nm), red line (acceptor emission, λ_{ex} = 480 nm), the blue line represents the fluorescence spectrum of **TPE-G1**, which was normalized according to the fluorescence intensity at 470 nm of the black line.

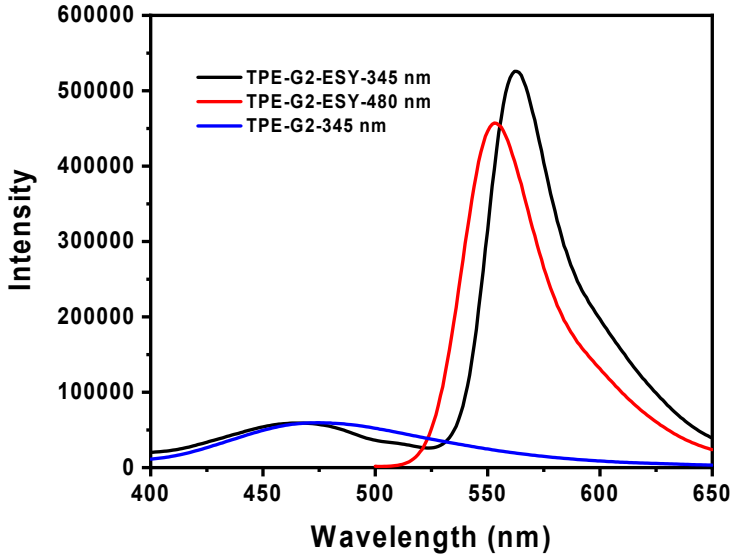

Figure S46. Fluorescence spectra of **TPE-G2-ESY** system ([TPE units]/[ESY] = 3/1) in DCM/ACN (v/v = 2/98) (black line, λ_{ex} = 345 nm), red line (acceptor emission, λ_{ex} = 480 nm), the blue line represents the fluorescence spectrum of **TPE-G2**, which was normalized according to the fluorescence intensity at 470 nm of the black line.

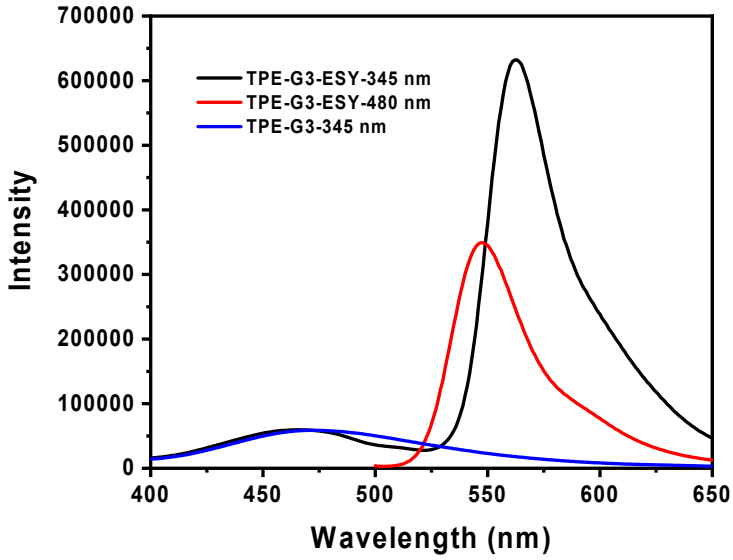

Figure S47. Fluorescence spectra of **TPE-G3-ESY** system ([TPE units]/[ESY] = 3/1) in DCM/ACN (v/v = 2/98) (black line, λ_{ex} = 345 nm), red line (acceptor emission, λ_{ex} = 480 nm), the blue line represents the fluorescence spectrum of **TPE-G3**, which was normalized according to the fluorescence intensity at 470 nm of the black line.

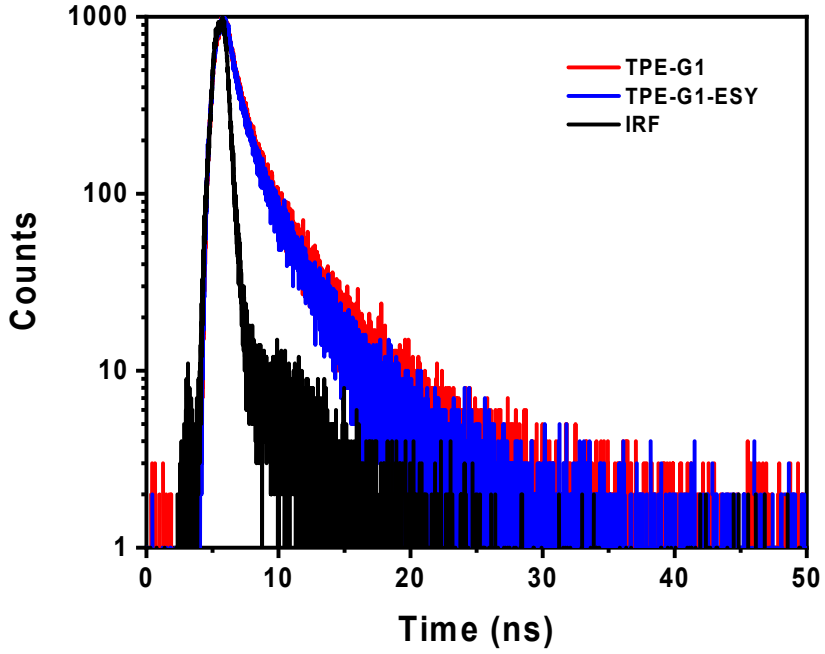

Figure S48. Time-resolved fluorescence decay curves for **TPE-G1** and **TPE-G1-ESY** system ([TPE units]/[ESY] = 3/1, in DCM/ACN with 98% ACN fractions, 375 nm excitation and 480 nm detection).

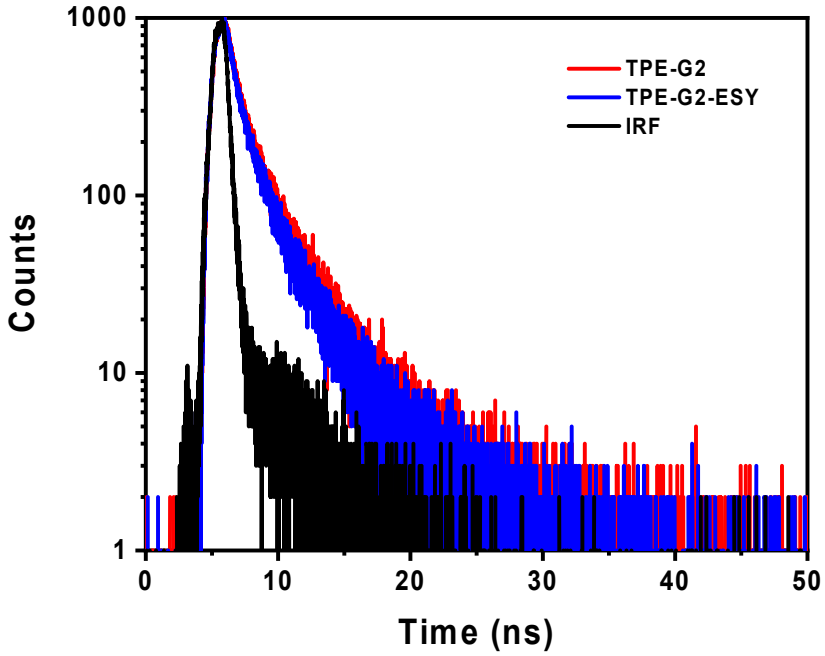

Figure S49. Time-resolved fluorescence decay curves for **TPE-G2** and **TPE-G2-ESY** system ([TPE units]/[ESY] = 3/1, in DCM/ACN with 98% ACN fractions, 375 nm excitation and 480 nm detection).

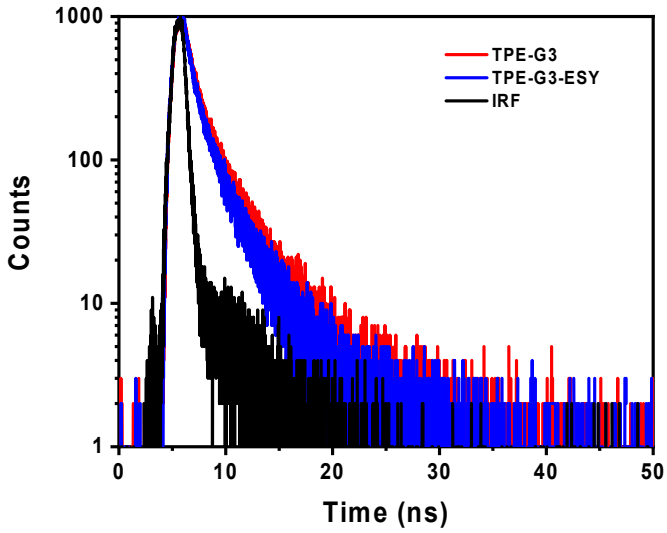

Figure S50. Time-resolved fluorescence decay curves for **TPE-G3** and **TPE-G3-ESY** system ([TPE units]/[ESY] = 3/1, in DCM/ACN with 98% ACN fractions, 375 nm excitation and 480 nm detection).

Table S2. The fluorescence lifetimes for **TPE-Gn-ESY** (n = 1, 2, 3) system ([TPE units]/[ESY] = 3/1, in DCM/ACN with 98% ACN fractions, 375 nm excitation and 480 nm detection).

Compound	τ_1	τ_2
TPE-G1	1.23	5.03
TPE-G1-ESY	1.15	4.60
TPE-G2	0.86	3.22
TPE-G2-ESY	0.85	3.11
TPE-G3	0.99	3.65
TPE-G3-ESY	0.94	3.53

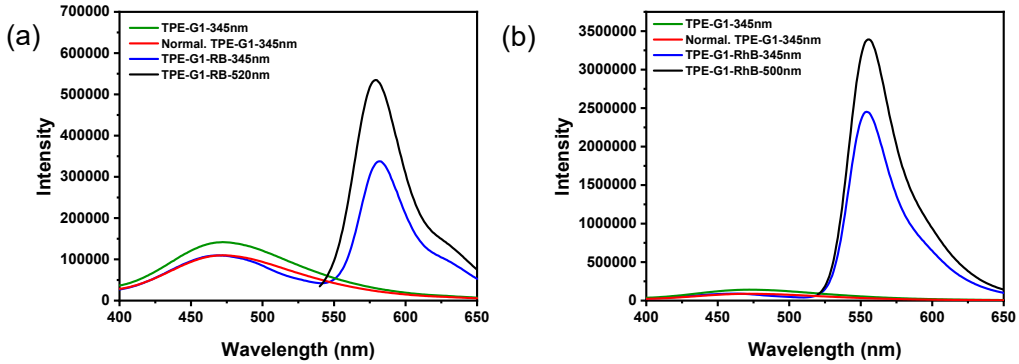

Figure S51. Fluorescence spectra of (a) **TPE-G1-RB** system in DCM/ACN (v/v = 2/98) (blue line, λ_{ex} = 345 nm), (black line, acceptor emission, λ_{ex} = 520 nm), the green line represents the fluorescence spectrum of **TPE-G1**, the red line represents the normalized fluorescence spectrum of **TPE-G1** according to the fluorescence intensity at 470 nm of the green line. Fluorescence spectra of (a) **TPE-G1-RhB** system in DCM/ACN (v/v = 2/98) (blue line, λ_{ex} = 345 nm), (black line, acceptor emission, λ_{ex} = 500 nm), the green line represents the fluorescence spectrum of **TPE-G1**, the red line represents the normalized fluorescence spectrum of **TPE-G1** according to the fluorescence intensity at 470 nm of the green line. The energy-transfer efficiencies between donor and acceptor were calculated to be: 22.9% (**TPE-G1-RB**), 37.3% (**TPE-G1-RhB**). The antenna effects were calculated to be: 0.59 (**TPE-G1-RB**), 0.71 (**TPE-G1-RhB**).

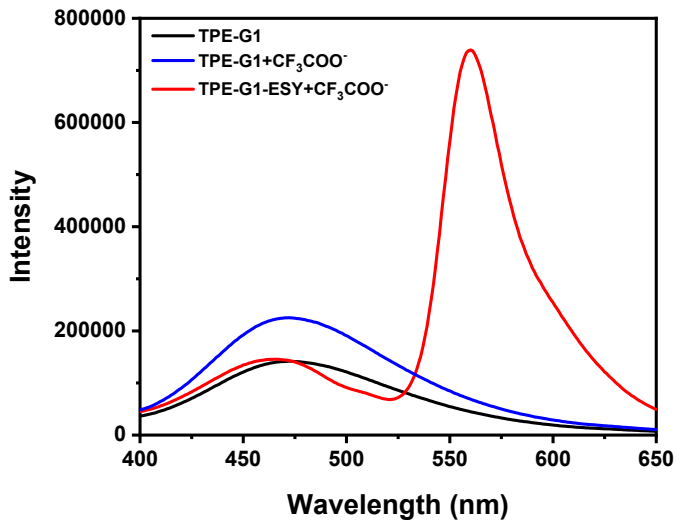

Figure S52. Fluorescence spectra of **TPE-G1**, **TPE-G1-ESY**, **TPE-G1-ESY+CF_3COO^-** system in DCM/ACN (v/v = 2/98, excitation at 345 nm). The energy-transfer efficiency between donor and acceptor was calculated to be 36.9%.

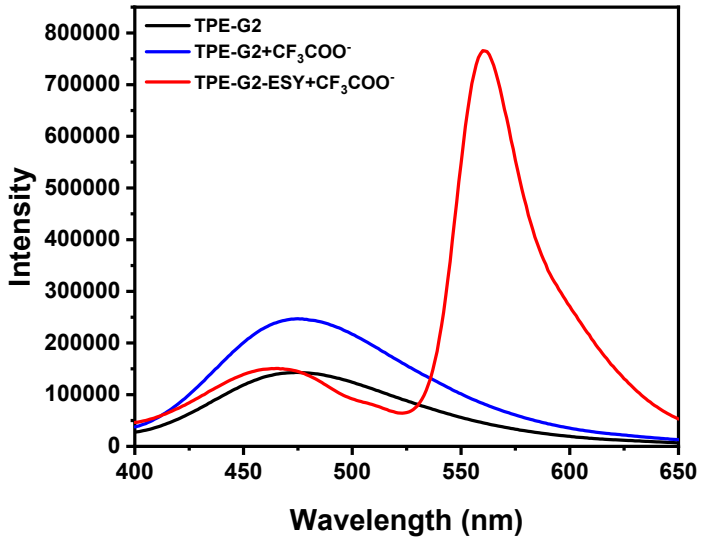

Figure S53. Fluorescence spectra of **TPE-G2**, **TPE-G2-ESY**, **TPE-G2-ESY+CF_3COO^-** system in DCM/ACN (v/v = 2/98, excitation at 345 nm). The energy-transfer efficiency between donor and acceptor was calculated to be 38.2%.

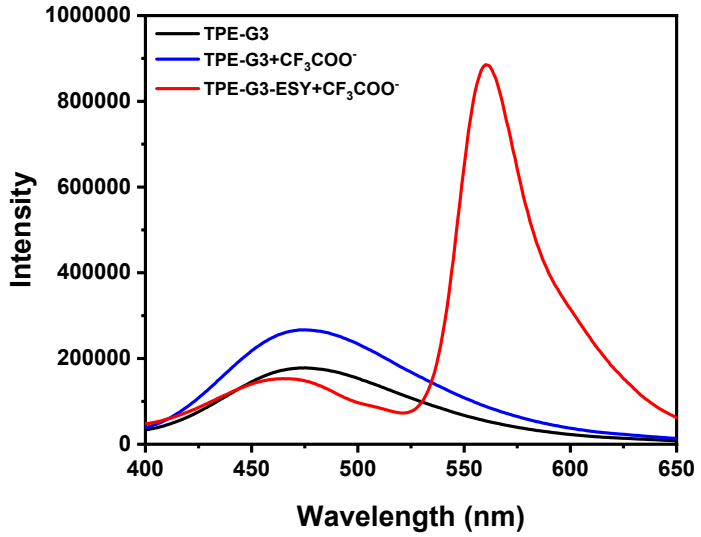

Figure S54. Fluorescence spectra of **TPE-G3**, **TPE-G3-ESY**, **TPE-G3-ESY+CF_3COO^-** system in DCM/ACN (v/v = 2/98, excitation at 345 nm). The energy-transfer efficiency between donor and acceptor was calculated to be 43.6%.

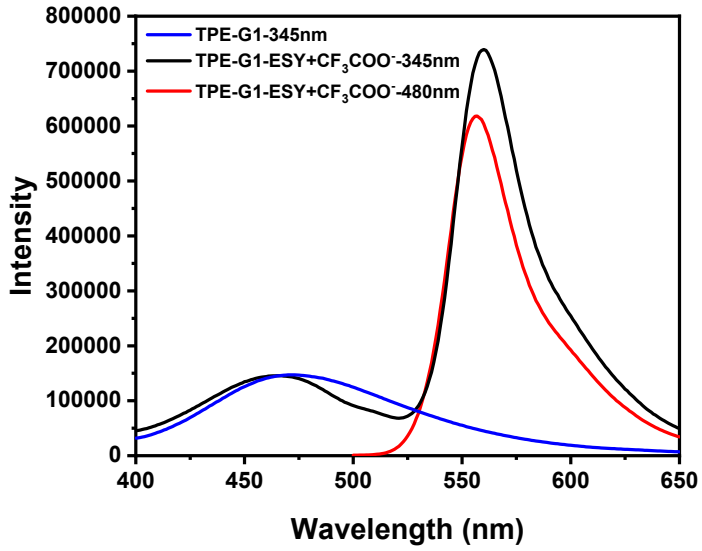

Figure S55. Fluorescence spectra of **TPE-G1-ESY+CF_3COO^-** system in DCM/ACN (v/v = 2/98) (black line, λ_{ex} = 345 nm), (red line, acceptor emission, λ_{ex} = 500 nm), the blue line represents the fluorescence spectrum of **TPE-G1**, which was normalized according to the fluorescence intensity at 470 nm of the black line. The antenna effect was calculated to be 1.13.

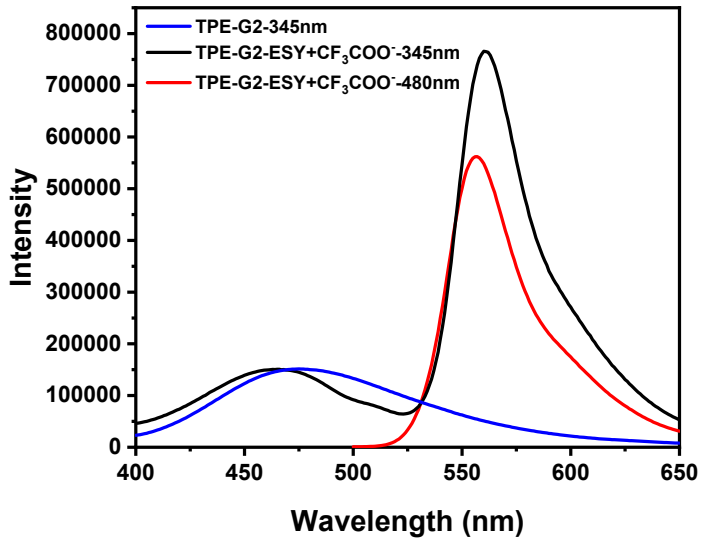

Figure S56. Fluorescence spectra of **TPE-G2-ESY+CF_3COO^-** system in DCM/ACN (v/v = 2/98) (black line, λ_{ex} = 345 nm), (red line, acceptor emission, λ_{ex} = 500 nm), the blue line represents the fluorescence spectrum of **TPE-G2**, which was normalized according to the fluorescence intensity at 470 nm of the black line. The antenna effect was calculated to be 1.27.

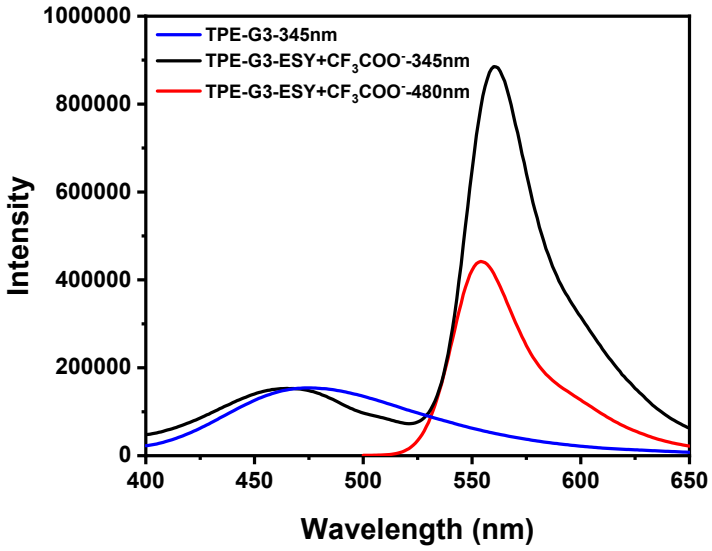

Figure S57. Fluorescence spectra of **TPE-G3-ESY+CF_3COO^-** system in DCM/ACN (v/v = 2/98) (black line, λ_{ex} = 345 nm), (red line, acceptor emission, λ_{ex} = 500 nm), the blue line represents the fluorescence spectrum of **TPE-G3**, which was normalized according to the fluorescence intensity at 470 nm of the black line. The antenna effect was calculated to be 1.88.

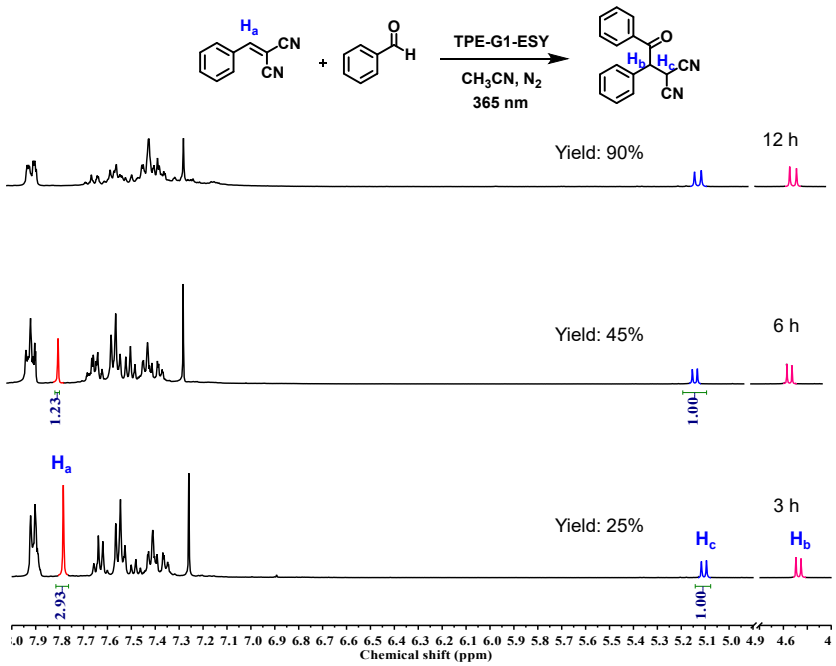

Figure S58. ^{1}H NMR spectra ($CDCl_3$, 298 K, 400 MHz) of photocatalytic reaction in the presence of **TPE-G1-ESY** as photosensitizer after irradiation at different time in ACN. The yields marked in the middle and bottom were determined from the crude ^{1}H NMR spectra, and the yield marked at the top was obtained after purification.

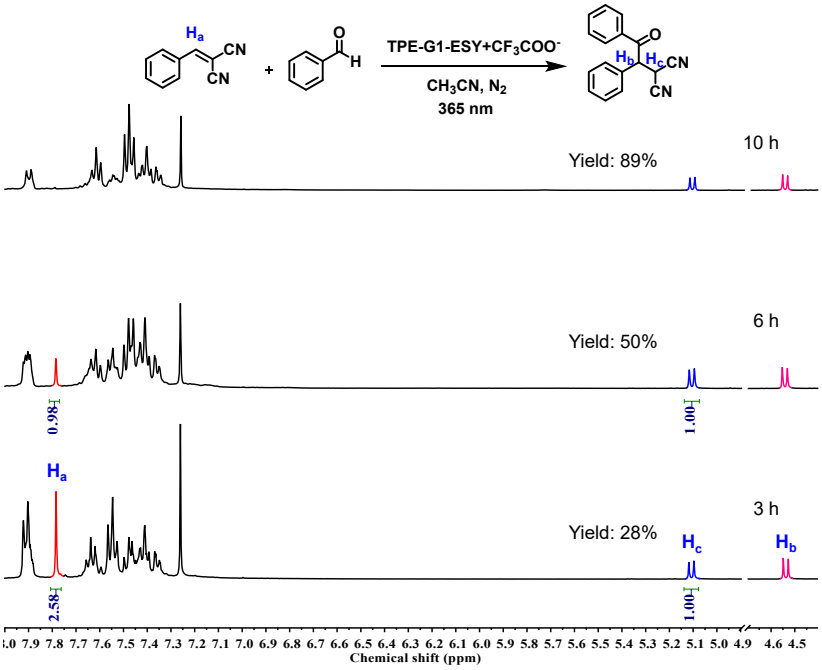

Figure S59. ^{1}H NMR spectra ($CDCl_3$, 298 K, 400 MHz) of photocatalytic reaction in the presence of **TPE-G1-ESY+CF_3COO^-** as photosensitizer after irradiation at different time in ACN. The yields marked in the middle and bottom were determined from the crude ^{1}H NMR, and the yield marked at the top was obtained after purification.

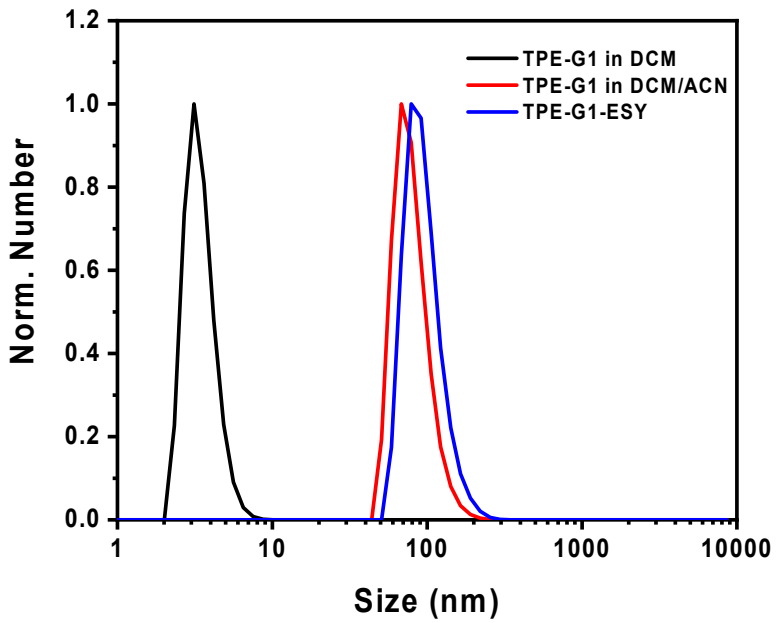

Figure S60. DLS data of **TPE-G1** and **TPE-G1-ESY** system ([TPE units]/[ESY] = 3/1) in DCM/ACN with 98% ACN fractions. The average hydrodynamic size of **TPE-G1** in DCM, **TPE-G1** in DCM/ACN and **TPE-G1-ESY** system was 3.6 ± 0.1 nm, 80.5 ± 0.3 nm and 95.5 ± 1.3 nm, respectively.

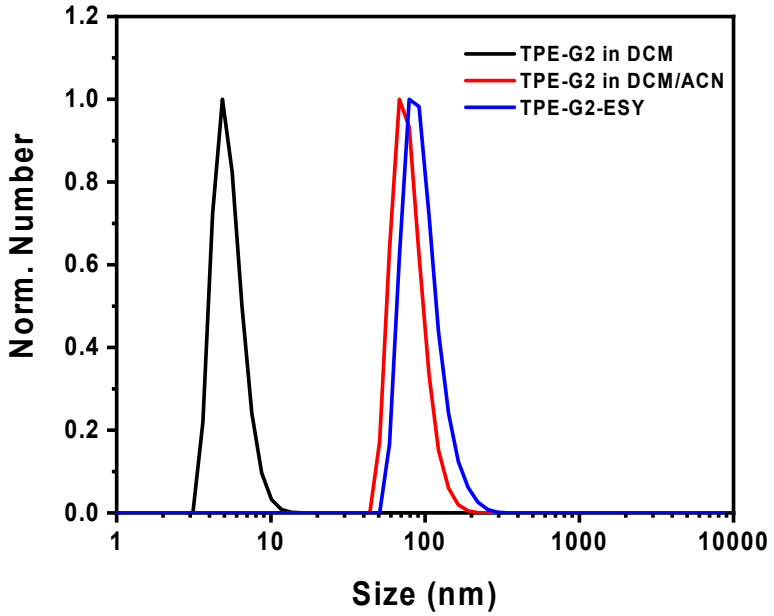

Figure S61. DLS data of **TPE-G2** and **TPE-G2-ESY** system ([TPE units]/[ESY] = 3/1) in DCM/ACN with 98% ACN fractions. The average hydrodynamic size of **TPE-G2** in DCM, **TPE-G2** in DCM/ACN and **TPE-G2-ESY** system was 5.6 ± 0.2 nm, 79.1 ± 1.1 nm and 96.8 ± 0.2 nm, respectively.

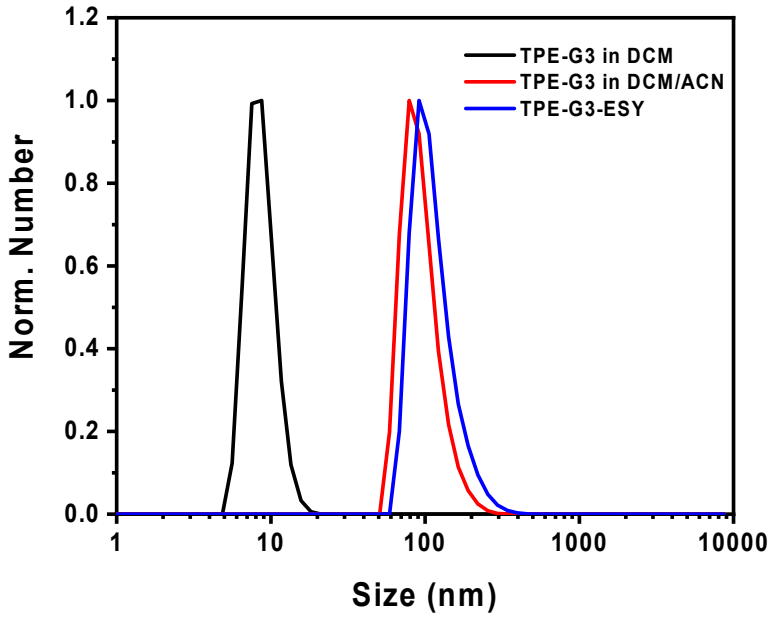

Figure S62. DLS data of **TPE-G3** and **TPE-G3-ESY** system ([TPE units]/[ESY] = 3/1) in DCM/ACN with 98% ACN fractions. The average hydrodynamic size of **TPE-G3** in DCM, **TPE-G3** in DCM/ACN and **TPE-G3-ESY** system was 8.7 ± 0.5 nm, 95.2 ± 1.5 nm and 114.9 ± 1.2 nm, respectively.

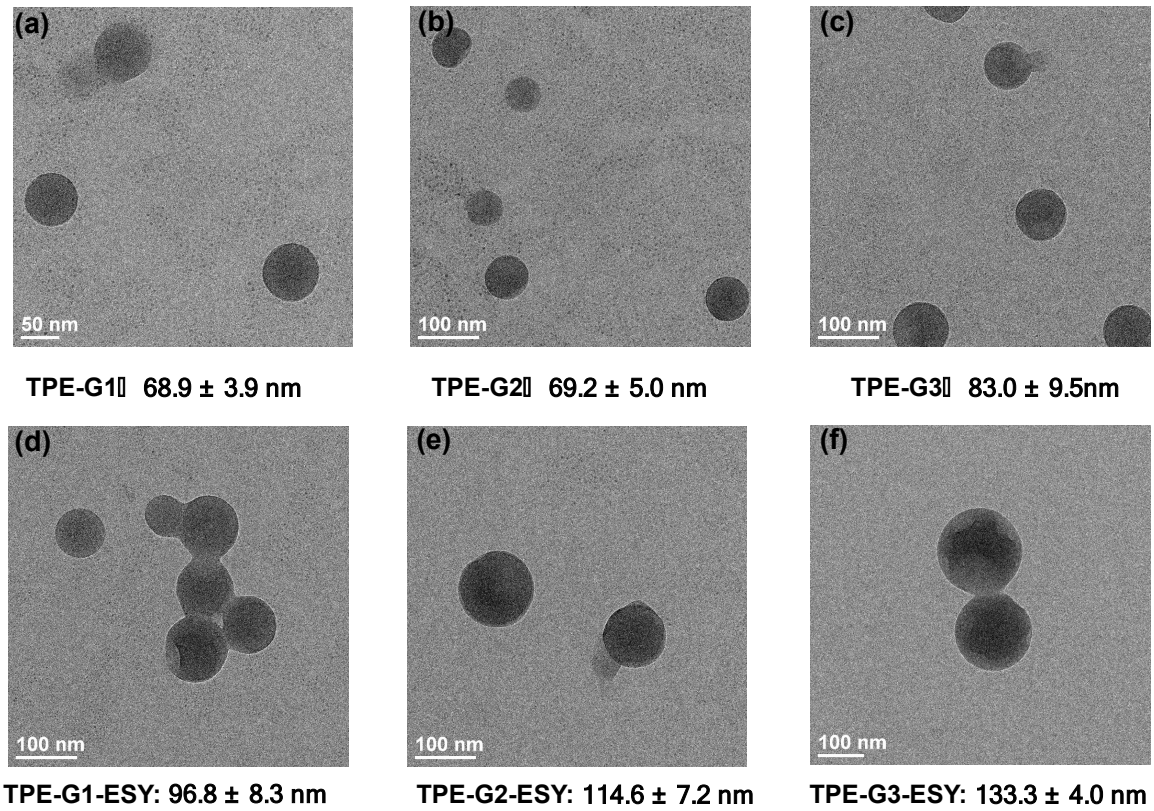

Figure S63. TEM image of (a-c) **TPE-Gn** (n = 1, 2, 3) and (d-f) **TPE-Gn-ESY** (n = 1, 2, 3) system ([TPE units]/[ESY] = 3/1) in DCM/ACN with 98% ACN fractions.

Section G. Photocatalysis study of artificial light-harvesting systems TPE-Gn-ESY (n = 1, 2, 3)

Scheme S5. Catalyst comparison data for the functionalization of inert C-H bonds.

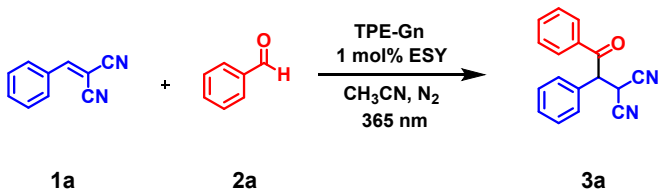

General procedure for C-H bond activation reactions of 2-benzylidenemalononitrile 1a with benzaldehyde 2a catalyzed by TPE-Gn-ESY (n = 1, 2, 3) as photocatalyst: The photocatalyst (1 mol% ESY relative to **1a**, TPE unit/ESY = 3/1), **1a** (0.1 mmol) and **2a** (0.3 mmol) were added into 2 mL CH_3CN. The reaction mixture with stirring was irradiated by a high intensity UV lamp (Analytik Jena, 365 nm, 100 W, REF 230 V-50/60 Hz) for 12 h under N_2 at room temperature. After the completion of the reaction (monitored by TLC), the solvent was removed by rotary evaporation and purified by column chromatography on silica gel using petroleum ether/dichloromethane (10:1) as eluent.

Table S3. Catalyst comparison data for the dehalogenation of α-bromoacetophenone.

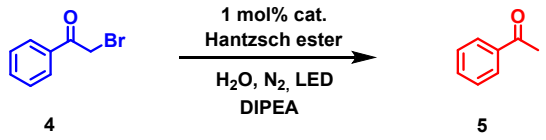

Entry	Catalyst	Time	Yield (%)
1	**No cat.**	2 h	20%
2	**ESY**	2 h	43%
3	**TPE-G1**	2 h	25%
4	**TPE-G1-ESY**	2 h	96%

α-Bromoacetophenone **4** (0.1 mmol, 20.0 mg), diethyl-2,6-dimethyl-1,4-dihydropyridine-3,5-dicarboxylate (0.1 mmol, 27.9 mg), photocatalyst (1 mol% ESY relative to **4**, TPE unit/ESY = 3/1) and N, N-diisopropylethylamine (DIPEA) (0.2 mmol, 25.8 mg) were added into 2 mL H_2O. The mixture was cooled by liquid nitrogen, degassed and purged with nitrogen for three times, and then irradiated by 12 W White LED at room temperature for corresponding time. After that, the mixture was diluted with diethyl ether (12 × 2 mL). The organic layer was collected and dried over Na_2SO_4 and concentrated. The solvents removed in vacuum and was purified by column chromatography on silica gel (PE: DCM = 30: 1) to get yellow liquid (11.5 mg), yield: 96%. ^{1}H NMR (400 MHz, $CDCl_3$) δ 7.95-7.97 (m, 2H), 7.55-7.59 (m, 1H), 7.45-7.49 (m, 2H), 2.61 (s, 3H).

Table S4. Catalyst comparison data for the aerobic oxidative conversion of benzothioamide into 1, 2, 4-thiadiazoles.

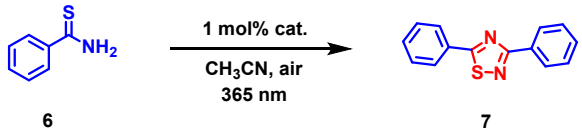

Entry	Catalyst	Time	Yield (%)
1	**No cat.**	2 h	none
2	**ESY**	2 h	28%
3	**TPE-G1**	2 h	trace
4	**TPE-G1-ESY**	2 h	86%

6 (0.1 mmol, 14.0 mg), photocatalyst (1 mol% ESY relative to **6**, TPE unit/ESY = 3/1) were added into 2 mL CH_3CN. The reaction mixture with stirring was irradiated by a high intensity UV lamp (Analytik Jena, 365 nm, 100 W, REF 230 V-50/60 Hz) for corresponding time under air at room temperature. After the completion of the reaction (monitored by TLC), the solvents removed in vacuum and was purified by column chromatography on silica gel (PE: EA = 10: 1) to get white solid (10.5 mg), yield: 86%. ^{1}H NMR (300 MHz, $CDCl_3$) δ 8.38-8.42 (m, 2H), 8.04-8.08 (m, 2H), 7.49-7.55 (m, 6H).

Table S5. Catalyst comparison data for the aerobic cross-dehydrogenative coupling reaction of N-phenyl-1, 2, 3, 4-tetrahydroisoquinoline with indole.

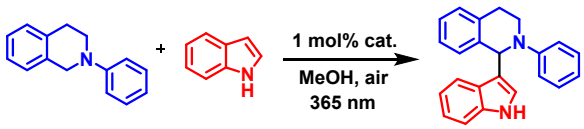

8 **9** **10**

Entry	Catalyst	Time	Yield (%)
1	**No cat.**	24 h	none
2	**ESY**	24 h	trace
3	**TPE-G1**	24 h	trace
4	**TPE-G1-ESY**	10 h	90%

The photocatalyst (1 mol% ESY units relative to **8**, TPE unit/ESY = 3/1), **8** (0.1 mmol) and **9** (0.3 mmol) were added into 2 mL CH_3OH. The reaction mixture with stirring was irradiated by a high intensity UV lamp (Analytik Jena, 365 nm, 100 W, REF 230 V-50/60 Hz) for corresponding time under air at room temperature. After the completion of the reaction (monitored by TLC), the solvents removed in vacuum and was purified by column chromatography on silica gel (PE: EA = 10: 1) to get white solid (29 mg), yield: 90%. ^{1}H NMR (400 MHz, Acetone-d_6) δ 10.05 (s, 1H), 7.54-7.56 (d, J = 8.0 Hz, 1H), 7.35-7.38 (m, 2H), 7.14-7.21 (m, 5H), 7.05-7.09 (m, 3H), 6.92-6.95 (m, 1H), 6.78-6.79 (m, 1H), 6.67-6.71 (m, 1H), 6.28 (s, 1H), 3.64-3.68 (m, 2H), 3.04-3.12 (dm, 1H), 2.86-2.92 (m, 1H).

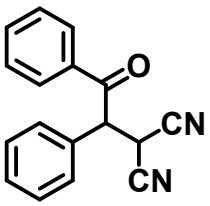

3a: Purified by column chromatography on silica gel (eluting with PE/DCM). The data were consistent with the previous report[S4]. ^{1}H NMR (400 MHz, $CDCl_3$): δ 7.89-7.91 (d, J = 8.0 Hz, 2H), 7.53-7.57 (t, J = 8.0 Hz, 1H), 7.35-7.43 (m, 7H), 5.10-5.12 (d, J = 8.0 Hz, 1H), 4.53-4.55 (d, J = 8.0 Hz, 1H).

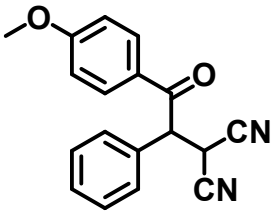

3b: Purified by column chromatography on silica gel (eluting with PE/DCM). The data were consistent with the previous report[S4]. ^{1}H NMR (400 MHz, $CDCl_3$): δ 7.87-7.89 (d, J = 8.0 Hz, 2H), 7.34-7.42 (m, 5H), 6.85-6.88 (d, J = 12.0 Hz, 2H), 5.04-5.06 (d, J = 8.0 Hz, 1H), 4.53-4.55 (d, J = 8.0 Hz, 1H), 3.82 (s, 3H).

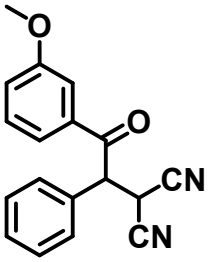

3c: Purified by column chromatography on silica gel (eluting with PE/DCM). ^{1}H NMR (400 MHz, $CDCl_3$): δ 7.29-7.46 (m, 8H), 7.08-7.10 (dd, J = 7.7, 2.5 Hz, 1H), 5.07-5.10 (d, J = 12.0 Hz, 1H), 4.52-4.54 (d, J = 8.0 Hz, 1H), 3.81 (s, 3H). ^{13}C NMR (126 MHz, $CDCl_3$) δ 192.82, 159.96, 135.14, 132.11, 130.08, 129.90, 129.89, 128.53, 121.82, 121.04, 113.38, 112.03, 111.46, 55.46, 54.97, 26.84. HRMS (ESI-TOF) m/z = 291.1130 [**3c** + H]$^+$ ($C_{18}H_{15}N_2O_2^+$ requires 291.1129).

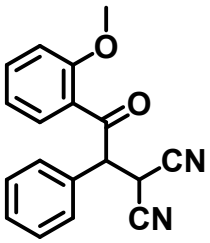

3d: Purified by column chromatography on silica gel (eluting with PE/DCM). ^{1}H NMR (400 MHz, $CDCl_3$): δ 7.83-7.86 (dd, J = 8.0, 4.0 Hz, 1H), 7.43-7.48 (m, 1H), 7.32-7.37 (m, 3H), 7.24 (m, 2H), 6.97-7.01 (m, 1H), 6.83-6.85 (d, J = 8.0 Hz, 1H), 5.37-5.39 (d, J = 8.0 Hz, 1H), 4.50-4.52 (d, J = 8.0 Hz, 1H), 3.83 (s, 3H). ^{13}C NMR (101 MHz, $CDCl_3$) δ 194.55, 158.40, 135.44, 131.97, 131.83, 129.31, 129.22, 129.10, 124.46, 121.12, 112.44, 111.91, 111.64, 58.01, 55.38, 26.68. HRMS (ESI-TOF) m/z = 291.1124 [**3d** + H]$^+$ ($C_{18}H_{15}N_2O_2^+$ requires 291.1129).

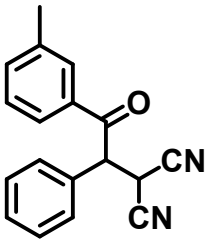

3e: Purified by column chromatography on silica gel (eluting with PE/DCM). ^{1}H NMR (400 MHz, $CDCl_3$): δ 7.75 (s, 1H), 7.65-7.67 (d, J = 8.0 Hz, 1H), 7.35-7.42 (m, 6H), 7.28-7.30 (d, J = 8.0 Hz, 1H), 5.09-5.11 (d, J = 8.0 Hz, 1H), 4.53-4.55 (d, J = 8.0 Hz, 1H), 2.36 (s, 3H). ^{13}C NMR (101 MHz, $CDCl_3$): δ 193.12, 138.96, 135.28, 133.86, 132.12, 130.06, 129.86, 129.71, 128.77, 128.55, 126.51, 112.11, 111.54, 54.80, 26.83, 21.35. HRMS (ESI-TOF) m/z = 275.1181 [**3e** + H]$^+$ ($C_{18}H_{15}N_2O^+$ requires 275.1179).

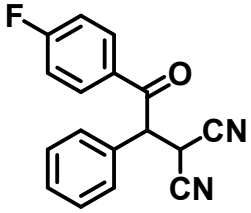

3f: Purified by column chromatography on silica gel (eluting with PE/DCM). ^{1}H NMR (400 MHz, $CDCl_3$): δ 7.91-7.95 (m, 2H), 7.41-7.46 (m, 3H), 7.33-7.35 (m, 2H), 7.06-7.11 (t, J = 10.0 Hz, 2H), 5.04-5.06 (d, J = 8.0 Hz, 1H), 4.51-5.53 (d, J = 8.0 Hz, 1H). ^{13}C NMR (126 MHz, $CDCl_3$): δ 191.41, 132.10, 132.03, 131.87, 130.18, 130.05, 128.53, 116.39, 116.21, 111.97, 111.36, 54.90, 26.82. ^{19}F NMR (376 MHz, $CDCl_3$) δ -101.69. HRMS (ESI-TOF) m/z = 279.0930 [**3f** + H]$^+$ ($C_{17}H_{12}FN_2O^+$ requires 279.0929).

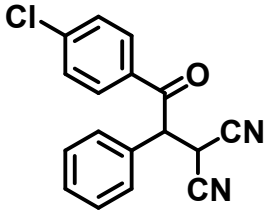

3g: Purified by column chromatography on silica gel (eluting with PE/DCM). ^{1}H NMR (400 MHz, $CDCl_3$): δ 7.82-7.84 (d, J = 8.0 Hz, 2H), 7.32-7.44 (m, 7H), 5.03-5.05 (d, J = 8.0 Hz, 1H), 4.50-4.52 (d, J = 8.0 Hz, 1H). ^{13}C NMR (101 MHz, $CDCl_3$): δ 191.83, 141.12, 132.06, 131.69, 130.58, 130.19, 130.08, 129.35, 128.52, 111.91, 111.31, 54.87, 26.77. HRMS (ESI-TOF) m/z = 295.0803 [**3g** + H]$^+$ ($C_{17}H_{12}ClN_2O^+$ requires 295.0633).

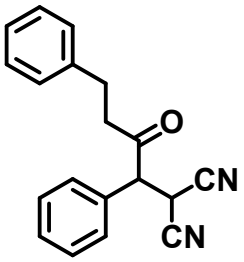

3h: Purified by column chromatography on silica gel (eluting with PE/DCM). The data were consistent with the previous report[S5]. ^{1}H NMR (400 MHz, $CDCl_3$): δ 7.39-7.43 (m, 3H), 7.19-7.24 (m, 3H), 7.12-7.14 (m, 2H), 7.04-7.06 (m, 2H), 4.32-4.35 (d, J = 8.0 Hz, 1H), 4.12-4.14 (d, J = 8.0 Hz, 1H), 2.83-2.95 (m, 2H), 2.70-2.75(m, 2H).

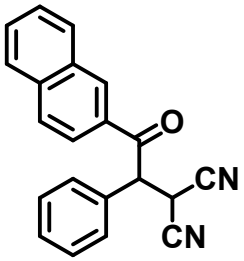

3i: Purified by column chromatography on silica gel (eluting with PE/DCM). ^{1}H NMR (400 MHz, $CDCl_3$): δ 8.42 (s, 1H), 7.93-7.95 (dd, J = 8.0, 2.0 Hz, 1H), 7.87-7.89 (d, J = 8.0 Hz, 1H), 7.82-7.85 (dd, J = 8.0, 4.0 Hz, 2H), 7.59-7.63 (m, 1H), 7.52-7.56 (m, 1H), 7.35-7.43 (m, 5H), 5.27-5.29 (d, J = 8.0 Hz, 1H), 4.60-4.62 (d, J = 8.0 Hz, 1H). ^{13}C NMR (101 MHz, $CDCl_3$): δ 192.92, 135.87, 132.16, 132.12, 131.67, 131.08, 130.04, 129.84, 129.76, 129.40, 128.88, 128.54, 127.76, 127.18, 123.98, 112.14, 111.56, 54.79, 26.86. HRMS (ESI-TOF) *m/z* = 311.1182 [**3i** + H]$^+$ ($C_{21}H_{15}N_2O^+$ requires 311.1179).

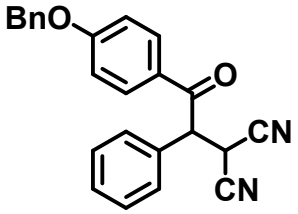

3j: Purified by column chromatography on silica gel (eluting with PE/DCM). ^{1}H NMR (400 MHz, $CDCl_3$): δ 7.87-7.89 (d, J = 8.0 Hz, 2H), 7.34-7.42 (m, 10H), 6.93-6.95 (d, J = 8.0 Hz, 2H), 5.09 (s, 2H), 5.03-5.05 (d, J = 8.0 Hz, 1H), 4.52-4.54 (d, J = 8.0 Hz, 1H). ^{13}C NMR (126 MHz, $CDCl_3$): δ 191.06, 163.43, 135.55, 132.34, 131.66, 131.57, 129.85, 129.62, 128.60, 128.35, 128.25, 127.29, 126.80, 114.85, 112.04, 111.47, 70.14, 54.44, 26.69. HRMS (ESI-TOF) *m/z* = 367.1442 [**3j** + H]$^+$ ($C_{24}H_{19}N_2O_2^+$ requires 367.1442).

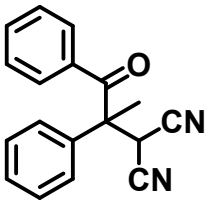

3k: Purified by column chromatography on silica gel (eluting with PE/DCM). ^{1}H NMR (400 MHz, $CDCl_3$): δ 7.41-7.52 (m, 8H), 7.28-7.32 (d, J = 8.0 Hz, 2H), 4.48 (s, 1H), 2.09 (s, 3H). ^{13}C NMR (101 MHz, $CDCl_3$): δ 197.40, 135.59, 133.44, 133.34, 130.08, 129.93, 129.84, 128.52, 126.69, 111.98, 111.78, 57.47, 35.06, 20.33. HRMS (ESI-TOF) *m/z* = 275.1180 [**3k** + H]$^+$ ($C_{18}H_{15}N_2O^+$ requires 275.1179).

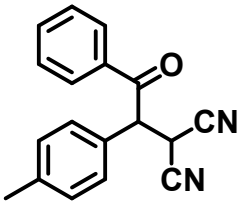

3l: Purified by column chromatography on silica gel (eluting with PE/DCM). The data were consistent with the previous report[S4]. ^{1}H NMR (400 MHz, $CDCl_3$): δ 7.91-7.92 (d, J = 4.0 Hz, 2H), 7.54-7.57 (t, J = 6.0 Hz, 1H), 7.40-7.44 (t, J = 8.0 Hz, 2H), 7.28-7.32 (t, J = 8.0 Hz, 1H), 7.13-7.20 (m, 1H), 5.06-5.08 (d, J = 8.0 Hz, 1H), 4.52-4.54 (d, J = 8.0 Hz, 1H), 2.34 (s, 3H).

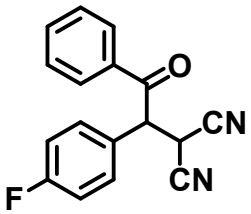

3m: Purified by column chromatography on silica gel (eluting with PE/DCM). The data were consistent with the previous report[S4]. ^{1}H NMR (400 MHz, $CDCl_3$): δ 7.87-7.89 (d, J = 8.0 Hz, 2H), 7.55-7.59 (t, J = 8.0 Hz, 1H), 7.41-7.44 (t, J = 6.0 Hz, 2H), 7.34-7.37 (dd, J = 8.0, 4.0 Hz, 2H), 7.10-7.14 (t, J = 8.0 Hz, 2H), 5.11-5.13 (d, J = 8.0 Hz, 1H), 4.51-4.53 (d, J = 8.0 Hz, 1H).

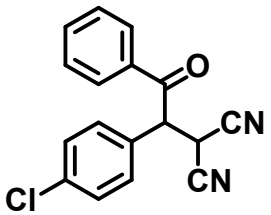

3n: Purified by column chromatography on silica gel (eluting with PE/DCM). The data were consistent with the previous report[S4]. ^{1}H NMR (400 MHz, $CDCl_3$): δ 7.86-7.88 (d, J = 8.0 Hz, 2H), 7.56-7.60 (t, J = 8.0 Hz, 1H), 7.40-7.45 (m, 4H), 7.29-7.31 (d, J = 8.0 Hz, 2H), 5.08-5.10 (d, J = 8.0 Hz, 1H), 4.51-4.53 (d, J = 8.0 Hz, 1H).

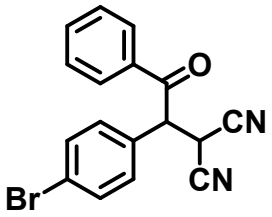

3o: Purified by column chromatography on silica gel (eluting with PE/DCM). The data were consistent with the previous report[S4]. ^{1}H NMR (400 MHz, $CDCl_3$): δ 7.86-7.88 (d, J = 8.0 Hz, 2H), 7.52-7.60 (m, 3H), 7.41-7.45 (t, J = 8.0 Hz, 2H), 7.23-7.25 (d, J = 8.0 Hz, 2H), 5.06-5.09 (d, J = 12.0 Hz, 1H), 4.51-4.53 (d, J = 8.0 Hz, 1H).

Scheme S6. Proposed Photocatalytic Mechanism for the C-H Bond Activation.

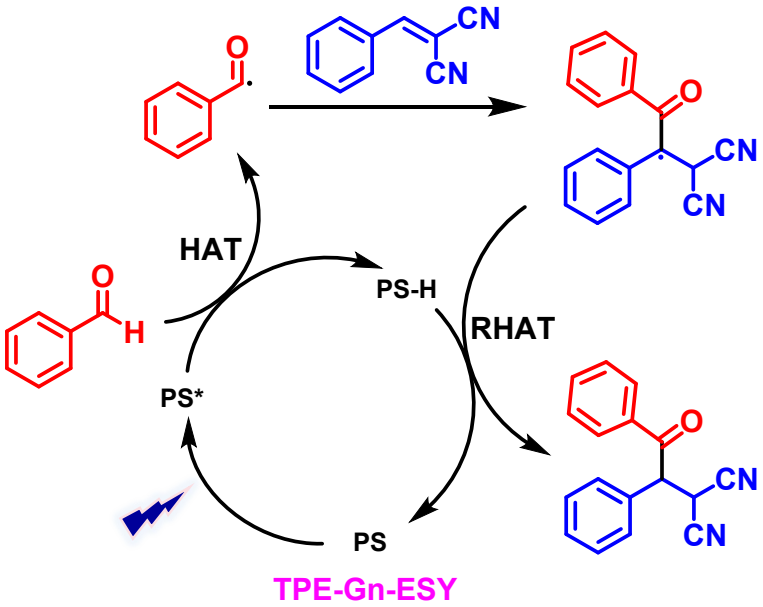

Section I. References

[S1] X.-Q. Wang, W. Wang, W.-J. Li, L.-J. Chen, R. Yao, G.-Q. Yin, Y.-X. Wang, Y. Zhang, J. Huang, H. Tan, Y. Yu, X. Li, L. Xu, H.-B. Yang, *Nat. Commun.* 2018, **9**, 3190.

[S2] X.-Q. Wang, W.-J. Li, W. Wang, J. Wen, Y. Zhang, H. Tan, H.-B. Yang, *J. Am. Chem. Soc.* 2019, **141**, 13923.

[S3] a) S. Guo, Y. Song, Y. He, X.-Y. Hu, L. Wang, *Angew. Chem. Int. Ed.* 2018, **57**, 3163; b) L. Xu, Z. Wang, R. Wang, L. Wang, X. He, H. Jiang, H. Tang, D. Cao, B. Z. Tang, *Angew. Chem. Int. Ed.* 2020, **59**, 9908; c) K. Acharyya, S. Bhattacharyya, H. Sepehrpour, S. Chakraborty, S. Lu, B. Shi, X. Li, P. S. Mukherjee, P. J. Stang, *J. Am. Chem. Soc.* 2019, **141**, 14565; d) H.-Q. Peng, L.-Y. Niu, Y.-Z. Chen, L.-Z. Wu, C.-H. Tung, Q.-Z. Yang, *Chem. Rev.* 2015, **115**, 7502.

[S4] L. Li, S. Guo, Q. Wang, J. Zhu. *Org. Lett*. 2019, **21**, 5462.

[S5] L. Capaldo, D. Merli, M. Fagnoni, D. Ravellelli, *ACS Catal.* 2019, 9, 3054.